JGR Atmospheres

RESEARCH ARTICLE
10.1029/2024JD043135

Variations in Tropical Cyclone Size and Rainfall Patterns Based on Synoptic-Scale Moisture Environments in the North Atlantic

K. D. Addington[1], S. E. Zick[2], K. M. Wood[3], C. J. Matyas[4], and K. Berislavich[1]

[1]Mississippi State University, Mississippi State, MS, USA, [2]Virginia Tech, Blacksburg, VA, USA, [3]University of Arizona, Tucson, AZ, USA, [4]University of Florida, Gainesville, FL, USA

Key Points:

- Tropical cyclones with abundant moisture located southeast of the center tend to have larger rain areas and more enclosed rainbands
- Tropical cyclones with dry air surrounding and to the southeast of the center have smaller rain areas with solid, compact convective precipitation
- Wind field size (R34, R64, radius of maximum wind (RMW), and radius of the outermost closed isobar (ROCI)) is not significantly different among tropical cyclones in the four moisture environments

Supporting Information:

Supporting Information may be found in the online version of this article.

Correspondence to:

S. E. Zick,
sezick@vt.edu

Citation:

Addington, K. D., Zick, S. E., Wood, K. M., Matyas, C. J., & Berislavich, K. (2025). Variations in tropical cyclone size and rainfall patterns based on synoptic-scale moisture environments in the North Atlantic. *Journal of Geophysical Research: Atmospheres*, *130*, e2024JD043135. https://doi.org/10.1029/2024JD043135

Received 11 DEC 2024
Accepted 29 APR 2025

Author Contributions:

Conceptualization: S. E. Zick, K. M. Wood, C. J. Matyas
Data curation: S. E. Zick, K. M. Wood
Formal analysis: K. D. Addington, S. E. Zick, K. M. Wood, K. Berislavich
Funding acquisition: S. E. Zick, K. M. Wood, C. J. Matyas
Investigation: K. D. Addington, S. E. Zick, K. Berislavich
Methodology: K. D. Addington, S. E. Zick, K. M. Wood, C. J. Matyas
Project administration: S. E. Zick

Abstract Prior research has shown that tropical cyclone (TC) size, which is integral in determining the spatial extent of TC impacts, is influenced by environmental wind shear and the overall moisture environment. This study considers North Atlantic TCs located within low to moderate wind shear and at least 100 km from major landmasses. An empirical orthogonal function (EOF) analysis is applied to distinguish moisture environments based on the spatial pattern of total column water vapor surrounding the TC. Using these EOF patterns, four separate categories (groups) are created. Principal component scores indicate the TC samples most contributing to each EOF pattern and ultimately determine the cases in each group. TC structural differences among the groups are compared using size metrics based on the wind and precipitation fields and shape metrics based on the precipitation field. These metrics are considered across a 48-hr window centered on the sample times evaluated in the EOF analysis. There are no statistically significant differences in the TC wind field size, but TCs with abundant moisture to the southeast have larger rain areas with more outer rainbands. TCs in a dry environment or with dry air southeast of the TC center have generally smaller rain areas and less closed rainbands than TCs with moisture to the southeast. Future work will investigate the physical processes contributing to these spatial differences in precipitation.

Plain Language Summary Previous research shows that hurricane size and structure is affected by environmental humidity and wind shear, which is a change of wind speed and/or direction with height in the atmosphere. This project explores hurricanes in lower wind shear environments to focus on how the humidity around them affects their wind and precipitation structure. Size and shape metrics that capture the spatial extent of a hurricane's wind and rain are applied to hurricanes in different humidity patterns. Within the four humidity patterns, the extent of hurricane winds is similar across all groups. However, hurricanes with more moisture to their southeast tend to be the largest in terms of overall rain area, and hurricanes that have drier air to their southeast are generally smaller with the most rainfall concentrated near the storm center. Given these results, future work should focus on the processes contributing to the size and shape differences observed among these moisture groups.

1. Introduction

Complex relationships exist between tropical cyclone (TC) characteristics, such as intensity and the size of the wind and rain fields, and conditions in the surrounding environment including moisture and vertical wind shear. TC size is integral in determining the spatial extent of TC impacts. Size is influenced by numerous factors including the overall moisture environment (Hill & Lackmann, 2009; Matyas, 2017; Wu et al., 2015; Ying and Zhang, 2012), exposure to environmental wind shear (Corbosiero & Molinari, 2002; Frank & Ritchie, 1999; Reasor, 2004), and the location of the TC center relative to vertical wind shear and moisture (Ge et al., 2013; Matyas, 2010). Additionally, higher relative humidity is associated with greater rainfall production in landfalling TCs (Feng & Shu, 2018; Jiang et al., 2008). Based on idealized modeling and case studies, it is generally accepted that TCs developing in a dry environment intensify more slowly and are smaller in size compared to those developing in a moist environment (Braun et al., 2012; Hill & Lackmann, 2009; Martinez et al., 2020; Tang & Emanuel, 2010; Wu et al., 2015; Ying and Zhang, 2012). Idealized simulations show that environmental relative humidity values of 80% within 100 km of the TC center result in larger storms and a lower central pressure (Hill & Lackmann, 2009) since these storms have better access to moisture and produce more rainfall (Matyas, 2017) and convection within the storm (Ying and Zhang, 2012). The location of dry air also affects TC intensity: dry air

Software: K. D. Addington, S. E. Zick, K. M. Wood
Supervision: S. E. Zick, K. M. Wood
Validation: S. E. Zick
Visualization: K. D. Addington, S. E. Zick, K. M. Wood
Writing – original draft: K. D. Addington, S. E. Zick
Writing – review & editing: K. M. Wood, C. J. Matyas

located within 100 km of the TC center slows intensification or leads to weakening (Braun et al., 2012), whereas dry air surrounding a storm (but more than 100 km from the TC center) can contribute to a stronger TC. Since dry air is not conducive to convection outside of the TC, there is less interaction between the TC and convection beyond the TC (Wu et al., 2015). In addition, the extent to which this dry air impacts the TC depends on TC intensity (Tang & Emanuel, 2010).

Environmental moisture can affect the inner core and outer regions of a TC in different ways. Weatherford and Gray (1988a, 1988b) define the inner core as the region extending from the TC center to 1° latitude (approximately 111 km radius) and the outer core as extending 1–2.5° (approximately 111–278 km) from the TC center. The inner and outer core are generally related in terms of size and wind shear-induced asymmetries but are distinguished by different processes (Chavas & Lin, 2016; Weatherford & Gray, 1988a). Specifically, the inner core is characterized by turbulence and upward motion whereas the outer core is characterized by atmospheric stability and widespread downward motion (Chavas & Lin, 2016). TC intensity (maximum sustained winds) increases when the inflow of angular momentum increases (Holland & Merrill, 1984; Ying and Zhang, 2012). However, outer core convection can lead to a decrease in inflow to the inner core, slowing intensification (Rogers et al., 2013; Shapiro & Willoughby, 1982; Weatherford and Gray, 1988b). Although theoretical models can predict both the inner and outer sizes (Chavas & Lin, 2016; Chavas et al., 2015), the physical mechanisms that lead to changes in inner and outer size are not the same (Chavas & Knaff, 2022; Weatherford & Gray, 1988a). Studies using modern satellite data sets have also shown that outer core size is only weakly correlated with intensity and intensity change (Chavas & Emanuel, 2010; Ruan & Wu, 2022). More recently, Wang et al. (2022) and Wang and Chavas (2024) introduced an analytical model for TC potential size that predicts the equilibrium outer radius of a TC based solely on potential intensity and environmental parameters such as sea surface temperature, the Coriolis parameter f, outflow temperature, and surface exchange coefficients of enthalpy and momentum. Although their analytical solution for potential size does not explicitly include environmental relative humidity, the model itself is based on air-sea thermodynamic disequilibrium, which depends on sea surface temperature and atmospheric humidity. In summary, numerous studies have found that the outer core wind field is strongly influenced by environmental variables such as large-scale moisture (e.g., Chan & Chan, 2018). Although the inner core is where the highest winds occur and thus where intensity is defined, outer core size is important in understanding the over-land damage potential of TCs because it affects the rainfall associated with a TC, the radius of gale-force winds, and even storm surge potential (Irish et al., 2008; Klotzbach et al., 2020; Powell & Reinhold, 2007; Wang & Toumi, 2016; Weatherford and Gray, 1988b).

Although the current study focuses on the relationship between environmental moisture and TC size, it is impossible to completely isolate the impacts of moisture from the impacts of wind shear because the large-scale wind and moisture fields are determined by the synoptic-scale environment (e.g., Berislavich, 2023). Wind shear can tilt the TC vortex and cause a shear-induced secondary circulation that disrupts the in-up-and-out motion of the original forced secondary circulation, a disruption that results in structural asymmetries and a potentially expanded extent of TC-related convection (Corbosiero & Molinari, 2002; Ge et al., 2013; Matyas, 2010; Riemer & Laliberté, 2015). Additionally, wind shear that is primarily from the south or southwest can connect Northern Hemisphere TCs to deep tropical moisture, thus increasing the amount of rainfall associated with a TC (Matyas, 2017). Some studies have shown that the wind shear direction can be important to the TC's evolution as well (Chen et al., 2021; Ge et al., 2013; Matyas, 2010). In the North Atlantic, for example, since midlatitude frontal systems advect dry air north and west of the TC center (Ge et al., 2013), easterly wind shear can tilt the storm's primary circulation toward this dry air, therefore allowing dry air to penetrate the core and slow development. However, in the case of westerly shear, the cyclonic vortex tilts such that areas of upward motion are aligned with ample moisture thus enhancing development (Ge et al., 2013). Wind shear also influences the distribution of convection and rainfall in TCs as well as TC size. For example, Halverson et al. (2006) note that wind shear leads to subsidence upshear and left of the shear vector, a setup which can potentially reduce TC size through warming and drying in the upshear quadrants of the storm, potentially reducing TC size. However, strong shear, especially out of the southwest, leads to convection downshear and slightly left of the primary shear vector, which expands the TC (Corbosiero & Molinari, 2002; Matyas, 2010).

Given the complex relationships between environmental moisture, wind shear, and TC intensity described above, this research focuses on TCs in lower wind shear environments to assess the relationship between environmental moisture and TC size. Previous research used idealized models and case studies to investigate the role of environmental moisture on TC size and structure. However, to our knowledge, there are no observational studies

spanning numerous TCs that focus on how TCs respond to various environmental moisture pattern configurations. The current study uses observations to measure TC size and shape and then compares metrics that capture these characteristics across various large-scale moisture environments, therefore filling an important gap in the literature by investigating the relationship between environmental moisture and TC size in real TCs. In practice, the environment tends to be described as "dry" or "moist," but we will not use this binary classification since the surrounding two-dimensional moisture pattern is often asymmetric. The following research question is investigated: how do TC size metrics and precipitation spatial attributes differ in varying moisture environments? Specifically, we explore the differences among TCs in varied moisture environments at a "central" time step as well as differences in the evolution of shape and size metrics from 24 hr before through 24 hr after the central time step to better understand how the moisture environment affects storm size and structure.

The goal of this research is to enhance our understanding of the relationship between environmental moisture and TC size and structure and to provide an observational study that can be used to compare the results from numerous observed TCs with the results from existing modeling and case studies. Though this study focuses on TCs when their centers are over water, the results will be valuable for coastal communities since previous research shows that initial TC size is related to future TC size (Chan & Chan, 2014; Knaff et al., 2014). Results from this research should support improved prediction of the extent of TC impacts, which may later contribute to improving communication tools among hurricane forecasters, emergency management agencies, and coastal communities.

2. Data

This study uses the following data sets: (a) The National Hurricane Center (NHC) best-track (HURDAT2) data set, (b) the Statistical Hurricane Intensity Prediction Scheme (SHIPS) data set, (c) the Extended Best Track data set, (d) the NASA Integrated Multi-satellitE Retrievals for Global Precipitation Measurement (GPM) (IMERG) precipitation product version 6, and (e) the fifth generation European Center for Medium-Range Weather Forecasts (ECMWF) atmospheric reanalysis (ERA5).

The HURDAT2 data set https://www.nhc.noaa.gov/data/#hurdat; Landsea & Franklin, 2013) provides the TC latitude and longitude, 1-min 10-m maximum sustained winds, minimum sea level pressure, and the "tropical" nature of the TC at six-hourly time intervals (Landsea & Beven, 2019). Time since genesis (here, the time since designated as a tropical depression, in hours) is calculated using HURDAT2 since the TC wind field is known to expand over the TC lifecycle (Knaff et al., 2014). Vertical wind shear is provided by SHIPS, listed as SHRD, which is computed over the 200–800-km annulus between 200 and 850 hPa. In SHIPS, the shear magnitude and direction are calculated from the GFS analysis fields after the TC vortex has been removed (DeMaria & Kaplan, 1994; SHIPS Predictor File, 2022; Trabing & Bell, 2020). The Extended Best Track data set (EBT; Demuth et al., 2006; Regional and Mesoscale Meteorology Branch, 2022) reports numerous parameters for TCs occurring between 1988 and 2021 beyond those in HURDAT2, including the radial extent of 34- (R34) and 64- (R64) knot winds by quadrant, radius of maximum wind (RMW), and radius of the outermost closed isobar (ROCI) (Regional and Mesoscale Meteorology Branch, 2022). For this study, R34 and R64 values are averaged over all quadrants, meaning that we consider the average wind field size and ignore asymmetries. Additional potential biases in EBT wind data include potentially larger errors in TCs far from land due to (a) reduced aircraft reconnaissance and (b) more uncertainty in model analyses for TCs in data-sparse regions (e.g., over remote oceans).

Total column water vapor (TCWV) from ERA5 (Guillory, 2022; Hersbach et al., 2020) is used as input to the empirical orthogonal function (EOF) analysis, a procedure discussed further in Section 3.1. Additionally, we use ERA5 10-m wind data to diagnose the outer wind radius of the TC, a process described in Section 3.2. Although the spatial resolution of reanalysis data sets tends to be too coarse to resolve the TC inner core and other mesoscale features (Aarons et al., 2021; Dirkes et al., 2023; Murakami, 2014; Schenkel & Hart, 2012; Zick and Matyas, 2015a, 2015b), their resolution is sufficient to explore large-scale environmental patterns that affect TCs (Dirkes et al., 2023; Murakami, 2014; Slocum et al., 2022).

The NASA IMERG version 6 precipitation data set (Huffman et al., 2020) provides global rain rate estimates from 2000 through 30 September 2021 using observations from the Global Precipitation Measurement (GPM) mission and Tropical Rainfall Measuring Mission (TRMM) as well as other satellites (NASA Global Precipitation Measurement, 2022). IMERG integrates data collected from a range of passive microwave sensors in low-earth orbit alongside geostationary infrared observations, and the Final Run version recommended for research

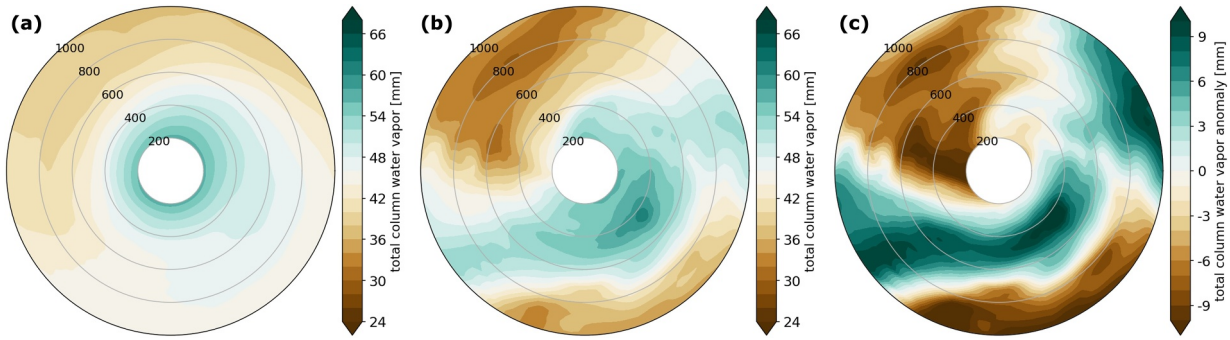

Figure 1. Total column water vapor [mm] plots of (a) the field averaged across all 00 UTC samples, (b) the pattern for Hurricane Alberto (AL032000), and (c) the anomaly for Hurricane Alberto.

purposes is calibrated to rain gauge measurements. The spatial resolution of this data set is 0.1° by 0.1°, and data are produced every 30 min (Huffman et al., 2020). For spatial analysis in this research, the IMERG data are interpolated to a 5 km × 5 km Lambert conformal grid. Li et al. (2022) show that the IMERG product tends to overestimate storm size and underestimate rain rates especially for small systems. These discrepancies are attributed to different precipitation types within the system and its position relative to local terrain. Because this study focuses on TCs located away from land, the effect of local terrain on the reliability of the IMERG product is likely minimized, but the effect of stratiform and convective precipitation types should be considered. Given the focus on spatial analysis and the interpolation of this data to a new grid, IMERG may have difficulty resolving the inner cores of TCs with small eyes. However, the IMERG data set is generally agreed to be the best product for estimating over-ocean TC precipitation and has been used for this purpose in previous studies (e.g., Rios Gaona et al., 2018).

3. Materials and Methods

3.1. Moisture Pattern Identification Using Empirical Orthogonal Function (EOF) Analysis

This study considers TCs in the mature stage (hurricanes with category 1+ intensity) during 2000–2021 located in an environment with weak to moderate vertical wind shear (≤20 kt) following thresholds defined in past work (e.g., Rios-Berrios & Torn, 2017). This study also limits the analysis to cases when the TC center is at least 100 km from major landmasses. Small islands with a maximum elevation of 100 m or less are not considered major land masses and therefore do not count toward this stipulation. Here, mature TCs have intensities of at least 64 kt for at least 24 hr. Next, we enforce a 48-hr constraint such that samples meeting the above criteria must be at least 48 hr apart for a given TC to ensure the independence of the inputs. There are 147 and 156 cases meeting these criteria for 00 UTC and 12 UTC, respectively. We evaluate 00 UTC and 12 UTC cases (or samples) separately to account for potential diurnal effects on the large-scale moisture field.

We perform EOF analysis using the python *eofs* package (Dawson, 2016) to identify the dominant moisture modes based on the large-scale spatial patterns surrounding these TCs. An EOF analysis, or principal component (PC) analysis (PCA), is used to reduce dimensionality of large data sets by creating new variables (principal components; PCs) that reveal dominant spatial patterns (Hannachi, 2004). Since ERA5 data are provided on a fixed latitude-longitude grid, storm-centered TCWV fields are converted to a fixed cylindrical coordinate system spanning 200–1,000 km from the center prior to conducting EOF analysis (e.g., Figure 1). Anomalies at each time step are computed relative to the total sample mean (Figure 1a), and grid points within 200 km of the TC center are excluded to focus on the environment surrounding the storm (Figures 1a–1c). To remove the influence of diurnal effects, the EOF analysis is performed twice: once on the subset of 00 UTC samples and once on the subset of 12 UTC samples. The resulting 00 and 12 UTC EOF patterns strongly resemble each other (Figure 2), so these samples are combined for all subsequent analyses.

Statistically significant EOF patterns are identified via the North test (North et al., 1982); here, the North test reveals EOFs 1–3 to be significant. However, this study focuses on EOFs 1 and 2 since these patterns represent commonly observed large-scale moisture patterns in the North Atlantic and explain 55% of the variance whereas EOF3 explains only 8% of the variance. Each TC sample has a corresponding PC score (or loading), which reveals

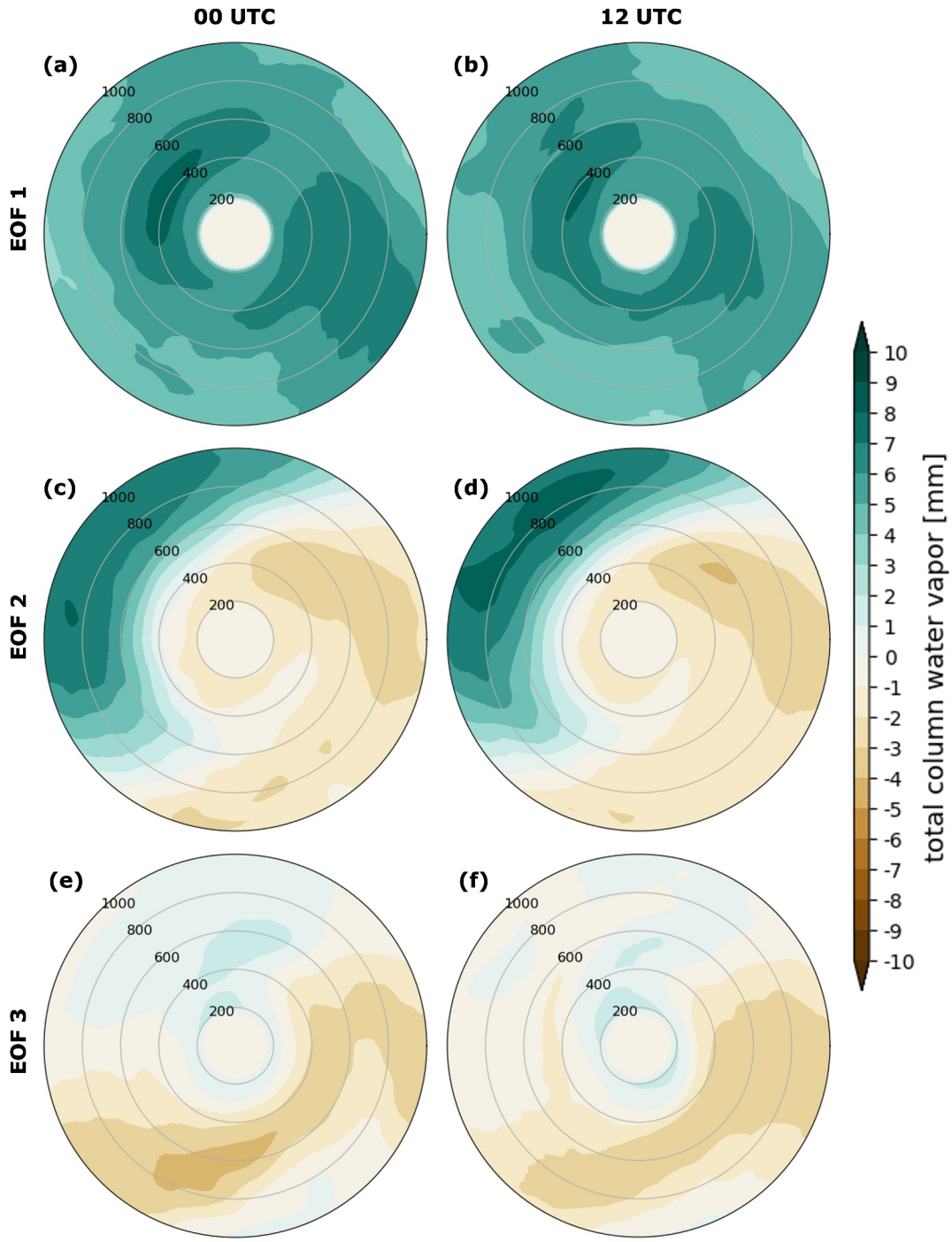

Figure 2. Plots showing total column water vapor (TCWV) anomaly patterns corresponding with empirical orthogonal functions (EOFs) 1, 2, and 3 (rows) at 00 and 12 UTC (columns). To obtain the amplitude represented by these EOFs in the original units of mm, we regress the principal components normalized to unit variance onto the original TCWV anomaly data set (e.g., Hannachi et al., 2007).

how well the sample matches the amplitude of that EOF, and the sign associated with that PC score represents whether the sample varies the same as or opposite to that EOF (Wilks, 2011). We then separate cases based on their normalized PC score by applying a threshold of ±0.75. To ensure unique sampling among our groups, we apply additional constraints: samples that meet the PC score threshold for multiple EOFs are removed, and if

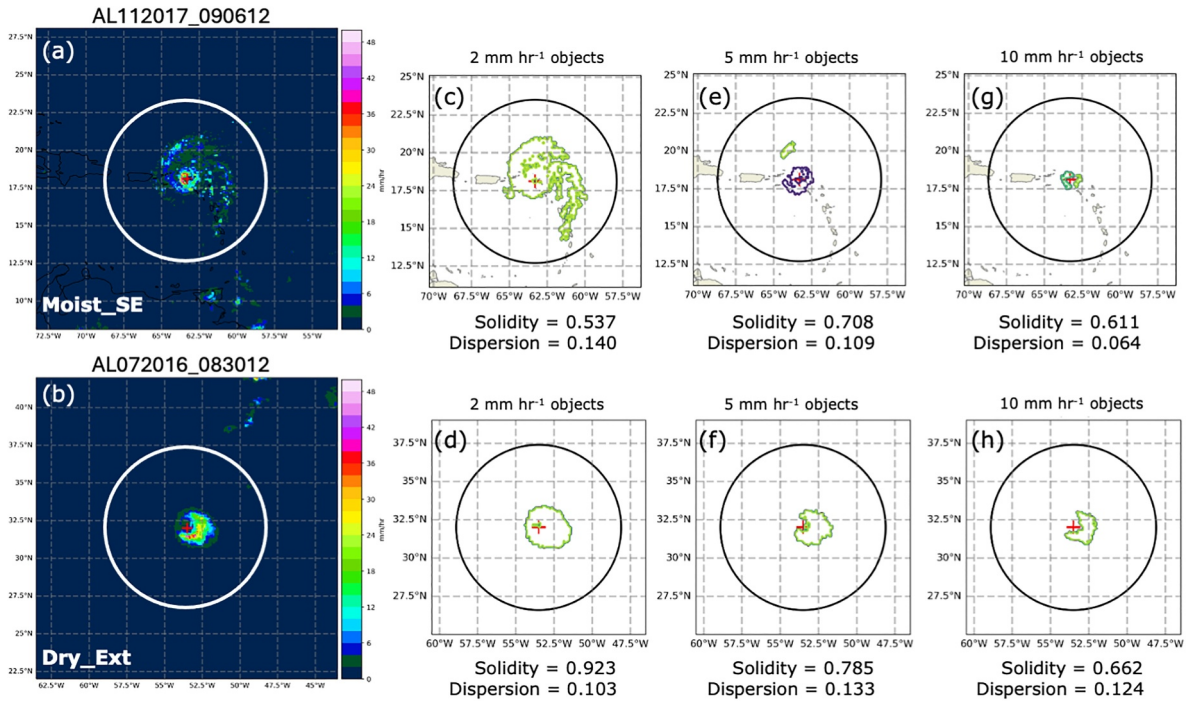

Figure 3. Example of the (a–b) precipitation field associated with a single TC "central" time step and the corresponding (c–d) 2 (d–f) 5, and (g–h) 10 mm hr^{-1} precipitation objects. The circles on each panel indicate 500-km search radius is shown by the white and black circles. The top row shows Hurricane Irma at 12 UTC 5 Sep 2017, a sample from the Moist_SE group. The bottom row shows Hurricane Gaston at 12 UTC 30 Aug 2016, a sample from the Dry_Ext group. Solidity and dispersion values for each time step and rain rate threshold are provided below the corresponding panels.

multiple samples from a single storm appear in the same group, only the sample with the highest PC score is retained. These additional criteria reduce the sample size to 75 cases from 61 unique storms.

3.2. Size Metrics

This study uses TC size parameters similar to those described by Kimball and Mulekar (2004) including ROCI, R34, R64, and RMW, which are provided by the EBT. Since impacts can extend beyond the TC rain field, these parameters help capture the overall size of the TC. Specifically, this study uses the ROCI and R34 values to examine effects of environmental moisture on the TC outer core and the RMW and R64 values to examine effects on the TC inner core. Wind radii are averaged over the entire storm, so some error may be introduced in asymmetric or small storms, a limitation discussed in Section 5. These values are evaluated over a 48-hr time period centered on the time steps used for EOF analysis to assess storm size for a given EOF pattern as well as the size evolution of those storms.

Beyond EBT data, we also consider outer wind radii, which we calculate using 10-m winds from ERA5. Specifically, we calculate the radii (in km) for the 6, 8, 10, and 12 m s^{-1} wind speed thresholds (hereafter R6, R8, R10, and R12), following Schenkel et al. (2017) and Gori et al. (2023). They noted that TC outer wind field size in reanalysis data sets (such as ERA5) is generally in good agreement with QuikSCAT satellite-derived wind field size for the period under consideration (2000–2021).

3.3. Shape Metrics

To identify precipitation objects, a 500-km search radius is applied to the 5 km × 5 km regridded IMERG fields to exclude precipitation features not directly related to the TC (Lonfat, 2004). Thresholding analysis is conducted by assigning a value of one (1) to rain rates greater than or equal to a threshold and a value of zero (0) to rain rates below that threshold (Figure 3). The 2 mm hr^{-1} rain rate delineates regions where stratiform cold rain processes dominate. The 5 and 10 mm hr^{-1} rain rate thresholds represent transitions between stratiform and convective precipitation. Typically, the 5 mm hr^{-1} rain rate refers to convective areas over water whereas the 10 mm hr^{-1} rain

rate represents areas of convection over land (Lau & Wu, 2003; Schumacher & Houze, 2003; Tokay et al., 1999). Since our study focuses on TCs over the ocean, we use the 5 mm hr^{-1} rain rate to designate convective precipitation, and the 10 mm hr^{-1} rain rate is used as an additional threshold above which convective processes are highly likely to be occurring. Lastly, all small objects within the search radius must be removed to focus on meso- to synoptic-scale structures such as rainbands rather than small-scale thunderstorms similar to prior studies (Bytheway & Kummerow, 2015; Stackhouse et al., 2023). Objects become smaller at higher rain rate thresholds, so a stricter minimum area threshold is implemented (e.g., Stackhouse et al., 2023). To be included in the object-based analysis, 2 mm hr^{-1} objects must have a minimum area of 15,000 km^2, 5 mm hr^{-1} objects must have a minimum area of 2,500 km^2, and 10 mm hr^{-1} objects must have a minimum area of 1,000 km^2.

The shape metrics in this study assign a value to precipitation fields to support quantitative comparisons of TC structure in varying environmental moisture patterns. All metrics are calculated for the three rain rate thresholds (2, 5, and 10 mm hr^{-1}) for the 48-hr period centered on the EOF analysis sample times. Area is defined as the two-dimensional coverage of precipitation objects within a prescribed distance of the TC center (Kirkland & Zick, 2019). In this research, the sum of areas (SOA) refers to the sum of precipitation object areas within 500 km of the TC center.

Closure is the proportion of the 360° around the TC center where precipitation exists (Kirkland & Zick, 2019). It is calculated as the number of 1-degree angles intersecting polygons divided by 360° (Equation 1), where a value of 1 suggests a fully enclosed arc whereas a value of 0.5 suggests a half-enclosed arc (Matyas & Tang, 2019; Stackhouse et al., 2023).

$$C = (\text{no. of } 1^\circ \text{ angles intersecting polygons})/360 \tag{1}$$

To calculate closure, annuli (radial bins) are explored within the defined search radius following Zick et al. (2022): C100 represents 0–100 km to focus on the TC inner core as defined by Weatherford and Grat (1988a); C200 represents 100–200 km to evaluate the intermediate region between the TC inner and outer core; and C300, C400, and C500 represent the 200–300, 300–400, and 400–500 km bins, respectively, to capture the TC outer core. Wind shear has been shown to reduce closure (Matyas & Tang, 2019; Matyas et al., 2018) by shifting and/or removing areas of precipitation, resulting in a less symmetric storm. Therefore, closure estimates support investigations of the impact of atmospheric moisture on TC size because enclosure of a TC center protects the TC from unfavorable wind shear and dry air. Midlevel dry air intrusion can lead to a weaker, narrower overturning secondary circulation, potentially leading to a smaller TC inner core (Alland et al., 2017), whereas dry air intrusion in outer regions of the TC can lead to expansion of the outer TC wind field (Wang & Toumi, 2019). Though shear is not allowed to exceed 20 kt for the samples included in the EOF analysis, it can breach this threshold in the latter portion of the 48-hr period being examined.

Dispersion (Equation 2) is a measure of centrality of precipitation around the TC center:

$$D = \sum_{i=1}^{NP} \frac{\text{Area}_i}{\sum_j^{NP} \text{Area}_j} \left(\frac{r_{\text{centroid},i}}{r_{\text{search}}} \right) \tag{2}$$

where NP is the number of polygons, r_{centroid} is the radial distance between the TC center and the object's centroid, and r_{search} is 500 km. A value near 1 suggests an asymmetric, or dispersed, storm whereas a value near 0 indicates a symmetric storm (Zick et al., 2022; Zick and Matyas, 2016). In the examples in Figure 3, the precipitation objects are centrally located with respect to the TC center, and the dispersion is low. The dispersion of the 2, 5, and 10 mm hr^{-1} rain rates highlights how each rain rate intensity may be affected by the surrounding moisture environment. Since dispersion measures the spatial layout of precipitation, this metric is related to closure. The dispersion metric can also provide insight into the interaction of TCs with fronts (Matyas & Tang, 2019) and/or degree of symmetry of the TC rainbands.

Solidity compares the area of a single precipitation object to the area of the entire rain field and is calculated by dividing the area of an object by the area of its convex hull (Equation 3).

$$S = \frac{\text{Area}}{\text{Convex Area}} \tag{3}$$

Values near zero suggest a more asymmetrical storm or a storm with outer rainbands (leading to empty areas) (e.g., Figure 3c). Smaller regions also tend to be more solid. A value of 1, however, suggests a circular, compact, and filled rain field (Zick et al., 2022; e.g., Figure 3f). In this project, a solidity metric helps us investigate TC structural differences because a TC with minimal banding will have higher solidity and a TC with extensive banding will have lower solidity (Figure 3).

3.4. Statistical Tests

A 95% confidence level ($p < 0.05$) is used for all statistical tests implemented in this study to compare TCs within moist and dry environments. The small sample size and non-normal distribution of TC size and spatial attributes requires a nonparametric test to evaluate the differences among the groups. The Kruskal-Wallis test is used to determine whether significant relationships exist among the four moisture groups (Kruskal & Wallis, 1952). Here, the null hypothesis is that all groups are similar in terms of the value of the metric measured. If significant relationships exist, the Dunn's multiple comparison test is applied to determine which groups(s) are significantly different (Dunn, 1964).

The Kruskal-Wallis test is also used to evaluate the significance in the temporal evolution of all spatial metrics during the 48-hr period of study. More specifically, we compare each spatial metric distribution for the five reference times: −24, −12, 0, +12, and +24 hr. Again, the null hypothesis is that the shape metric values are similar for the five time periods. A 5% significance level ($p < 0.05$) indicates that there are differences among the time periods, although it does not indicate which time period is different. If such a difference is indicated by the Kruskal-Wallis test, we apply the Dunn's multiple comparison test to determine which time period or pairs of time periods are significantly different from one another.

4. Results and Discussion

4.1. EOF Analysis Results

From the EOF analysis, we identify four categories of moisture patterns, which are named according to the geographic distribution of moisture surrounding the TC (Figure 4). Two EOF1 moisture fields are generated by adding (PC1+) and subtracting (PC1−) the EOF1 TCWV anomaly pattern (Figures 2a and 2b) to the TCWV mean field, and two EOF2 moisture fields are generated in a similar manner with the EOF2 TCWV anomaly pattern (Figures 2c and 2d). For all moisture patterns, we calculate the mean TCWV within 200–1,000 km of the TC center to help identify the environment as generally "moist," "moderate," or "dry." PC1+ (Moist_SE) is characterized by a moist anomaly to the southeast of the TC center; it is the most moist environment with 52.0 mm average TCWV. PC1- (Dry_Ext) is characterized by a dry environment around the entire storm with 37.8 mm average TCWV. PC2+ (Dry_NW) has dry air to the northwest of the TC center, and PC2- (Dry_SE) has dry air to the southeast of the TC center. The Dry_NW and Dry_SE environments have similar average TCWV with 47.7 and 46.1 mm, respectively. However, the spatial distribution of that moisture varies with respect to the cardinal direction of the driest air (NW vs. SE) and also the degree of symmetry (with Dry_NW being more asymmetric). Based on average TCWV values, we can consider Moist_SE to be a moist environment, Dry_Ext to be a dry environment, and the Dry_NW and Dry_SE to be moderate environments. The number of cases in each group is as follows: Moist_SE: 21, Dry_Ext: 13, Dry_SE: 21, and Dry_NW: 20.

The moisture environments described above resemble those found by Matyas et al. (2025), which applied a deep learning approach (a convolution autoencoder) and *k*-means cluster analysis to identify spatial patterns of TCWV around North Atlantic hurricanes. Their study found similar moisture patterns even though their methods and input TC cases were different, lending confidence to the results above. Like in this study, the inputs to the convolution autoencoder are ERA5 TCWV fields, but they explored all 2000–2021 North Atlantic hurricanes with no constraints on vertical wind shear, distance to land, or time between their 4,652 samples. Of the four distinct moisture patterns they identified, Cluster 1 (moderate moisture symmetrical) is similar to Dry_SE with 18 of the 21 TC samples coinciding with that cluster. Moist_SE and Dry_NW match quite well with cluster 2 (high moisture symmetrical) (17/21) and cluster 4 (high moisture asymmetrical) (18/20), respectively. Their cluster 3 (low moisture asymmetrical) lacks a clear counterpart in our results, likely due to the higher wind shear that these TCs experience (average > 23 kt). Our Dry_Ext group is the only environment that does not closely correspond with any of their clusters: six of the 13 fall within their cluster 1 and seven fall within their cluster 3. Note that their cluster 3 was their driest and had lower amounts of moisture with a 200–1,000-km average value of 33.4 mm

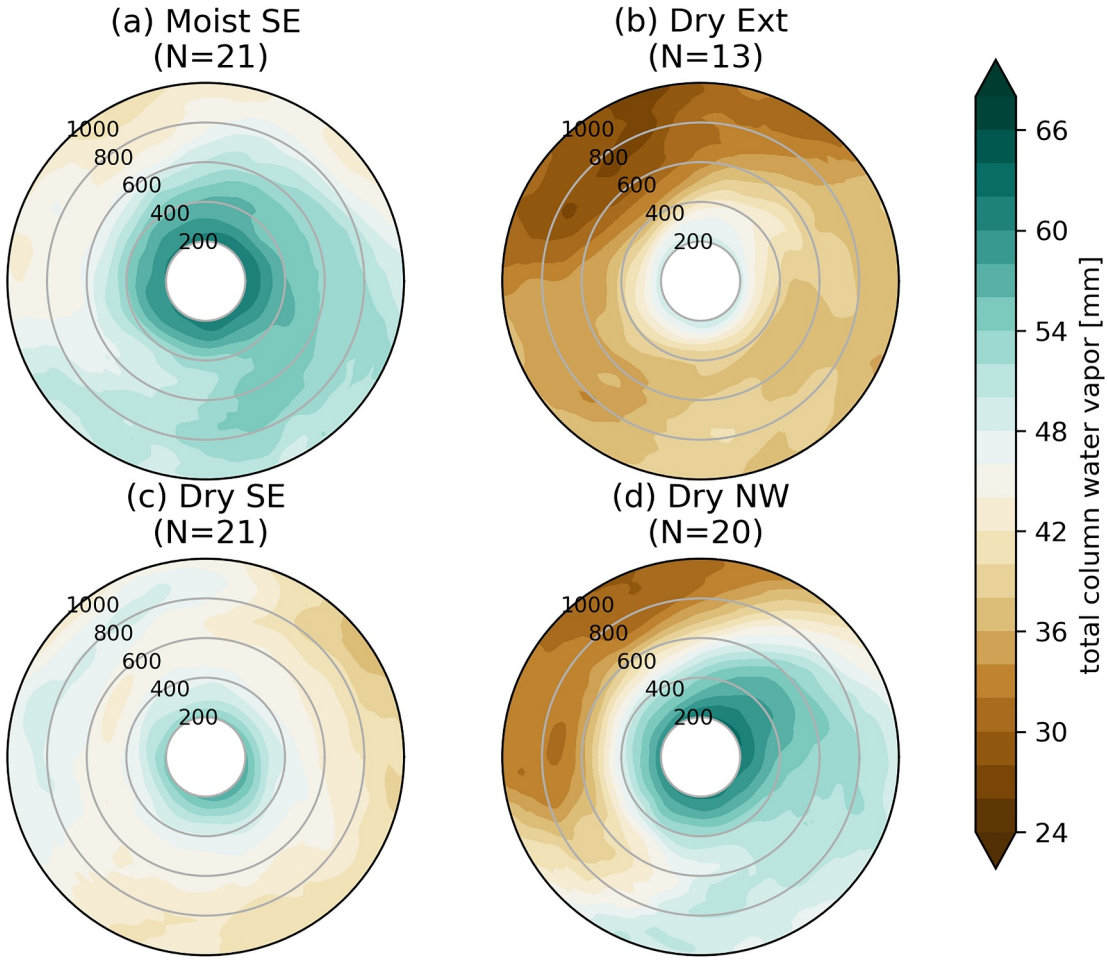

Figure 4. Total column water vapor (TCWV) patterns for the four groups created by compositing the TCWV for TC time steps meeting criteria for each group. Each group is named according to the moisture distribution, and sample sizes are included in parentheses.

compared to 38.1 mm in the current study. Overall, the similarities in three of the four moisture environments (and their geographic distributions) in this study suggest that the moisture environments we identified are robust even when a larger TC sample is considered.

Some geographic differences exist among the samples examined in this study (Figure 5). Most notably, cases within the Dry_Ext group are located farther north (Figure 5), clustered around 30°N latitude, compared to the other groups. Based on the Dunn's multiple comparison test, the Dry_Ext group is located significantly farther north than the Moist_SE ($p < 0.0001$) and Dry_NW ($p < 0.001$) groups, and the Dry_SE group is located slightly farther north than the Moist_SE group ($p < 0.05$). Longitudinally, Moist_SE TCs are located slightly farther west than the Dry_Ext group, which is generally confined to longitudes east of 65°W. Additionally, numerous Moist_SE and Dry_NW cases are located in the Gulf of Mexico and Caribbean Sea whereas there are no Dry_SE or Dry_Ext cases in this region (Figure 5). Dry_SE environments appear to be uncommon west of 75°W, although there are no statistically significant differences in the longitudes of this group compared with other groups (Figure 6). Dry_NW and Moist_SE cases have a larger zonal spread (~60°) than Dry_Ext and Dry_SE cases (~35°). Latitudinal differences among the groups could contribute to size and structure differences and will be discussed in Section 4.2.

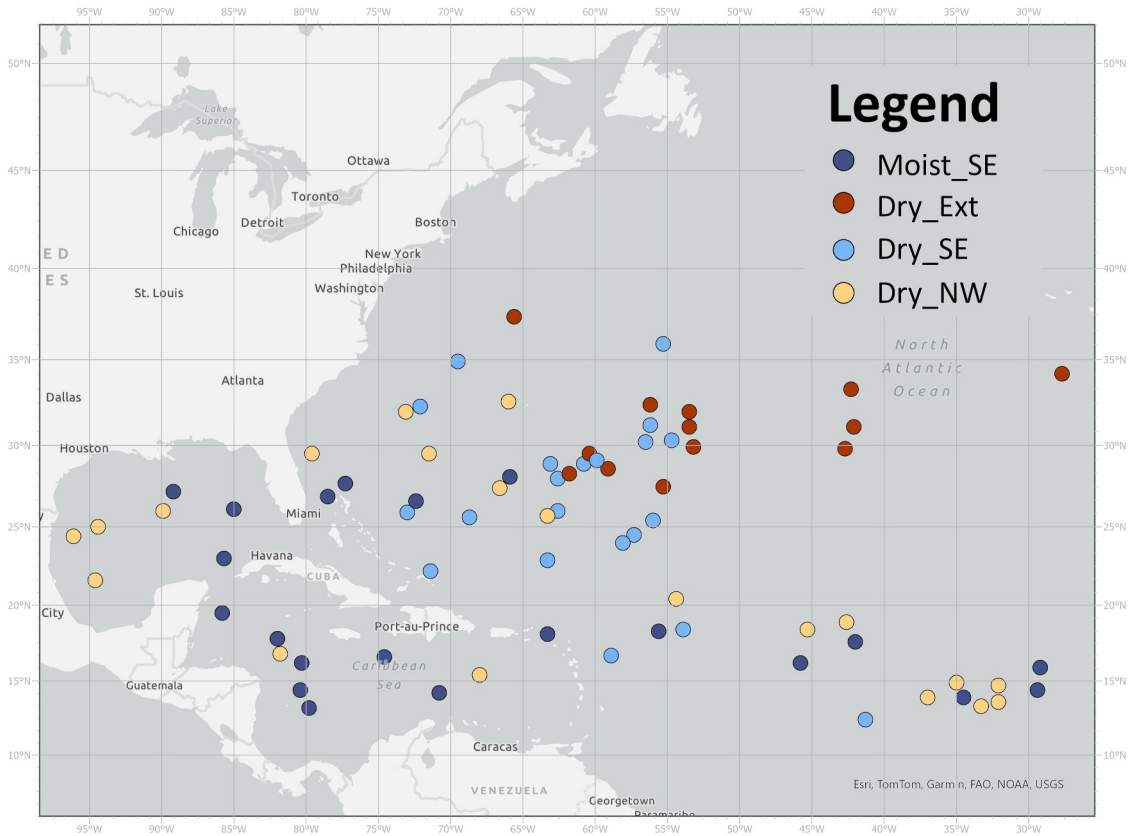

Figure 5. Map showing the locations of TC cases included in each group.

4.2. TC Characteristics by Moisture Environment

4.2.1. TC Size and Intensity Metrics

A correlation matrix is used to investigate the relationships between the size and shape metric variables and shows that these variables are not independent of each other (Table S1 in Supporting Information S1). This research focuses on relationships with a moderate to strong correlation (Pearson's $r > 0.6$). The RMW is not strongly associated with any other metric investigated here (Table S1 in Supporting Information S1). R34 is associated

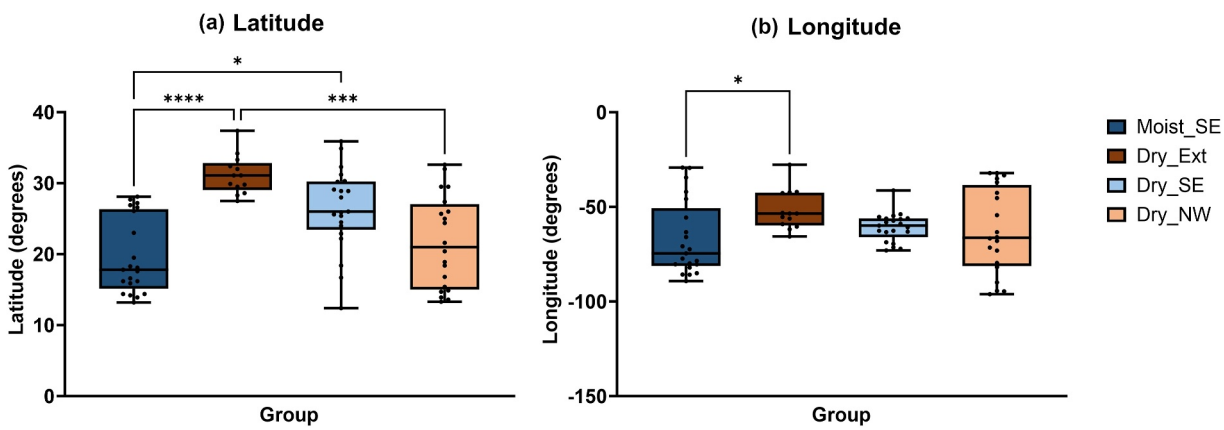

Figure 6. Box plots showing the latitudes and longitudes for four moisture environments. All box plots display the median and interquartile range (IQR), and the whiskers extend from the edges of the box to show the range of the data including any outliers. Dots represent all data values in the sample. The number of asterisks indicates statistical significance (*$p < 0.05$; **$p < 0.01$; ***$p < 0.001$ ****$p < 0.0001$).

Table 1
Results From the Kruskal-Wallis Test (p-Values) for Maximum Sustained Winds, MSLP, Radius of Maximum Wind, Radius of the Outermost Closed Isobar, R64, R34, R12, R10, R8, and R6 Compared Between Each Moisture Group

Size/Intensity metric	Kruskal-wallis test *p*-value
Maximum Sustained Winds	0.0988
MSLP	0.1296
RMW	0.6678
R64	0.5563
R34	0.8524
ROCI	0.3338
R12	0.4444
R10	0.6971
R8	0.4503
R6	0.0791

with the outer core of a TC and is moderately correlated with ROCI values (Table S1 in Supporting Information S1). Since hurricane-force winds are constrained to the area near the eye of the storm, we expect R64 to be most associated with the inner core of the storm, and indeed, R64 is only moderately correlated with R34 and MSLP (Table S1 in Supporting Information S1).

Though we did not find statistically significant differences in TC size among groups (Table 1, Figure S1 in Supporting Information S1), TCs in the Dry_NW and Dry_SE groups have slightly larger RMWs and more skewed distributions of RMW than TCs in the Moist_SE and Dry_Ext groups (Figure S1 in Supporting Information S1). Additionally, TCs in the Dry_Ext group have the smallest R64 values and the smallest range of R64 values (Figure S1 in Supporting Information S1). We also explore ROCI in addition to wind radii because ROCI concerns the pressure field rather than the wind field. Since pressure and wind are closely related, ROCI offers yet another way of comparing TC size. However, ROCI median values are similar across all four moisture environments (Table 1, Figure S1 in Supporting Information S1). In comparing our median size values to those of hurricanes from Kimball and Mulekar (2004), we find that our hurricanes are smaller compared to hurricanes in their study. We also find that our R34 values are lower than those in Matyas et al. (2025), who included hurricanes experiencing higher vertical wind shear and located at higher latitudes. Thus, the smaller range of hurricane sizes in our sample could partially explain the lack of significant differences among our four groups.

When we explored outer wind radii (R6, R8, R10, and R12), the differences among moisture groups were not statistically significant at a 95% confidence interval. Physically, TCs in the Dry_SE group have the smallest R6 and the smallest ROCI (Figure S1 in Supporting Information S1), which may be related to these cases occurring within comparatively dry environments (e.g., Chan & Chan, 2018; Hill & Lackmann, 2009; Matyas et al., 2025). Note that R6 is significant at a 90% confidence interval and R10 through R6 have decreasing *p*-values, which suggest that the R6 relationship could become significant in a larger sample of TCs.

4.2.2. Shape Metrics

In this study, shape metric calculations use satellite-derived rain rates to quantify storm size and structure. The sum of areas (SOA) is a basic measure of the TC rain field area (Section 3.3). Closure, solidity, and dispersion offer further insight beyond storm size and help to describe and measure structure within a storm. We evaluate each of the below shape metrics at three rain rate thresholds (2, 5, and 10 mm hr^{-1}).

4.2.2.1. Sum of Areas (SOA)

The SOA of all precipitation objects is largest for TCs in the Moist_SE group (Figure 7). A larger 2 mm hr^{-1} SOA is typically associated with a larger 5 and 10 mm hr^{-1} SOA (Table S1 in Supporting Information S1). As noted in Section 2.3, the 5 and 10 mm hr^{-1} rain rates represent transition areas and areas of convective precipitation, respectively, and areas of convection are typically located closer to the TC center. The SOA for convective areas (10 mm hr^{-1} rain rate) is largest in the Moist_SE group (Figure 7) and associated with higher closure in the inner regions of the TC (Table S1 in Supporting Information S1), which suggests that most of these precipitation objects are present in the inner region of the storm.

The Dry_Ext group is significantly smaller than the Moist_SE and Dry_NW groups at all rain rates. Additionally, the Dry_SE group is significantly smaller than the Moist_SE group at the 2 mm hr^{-1} rain rate (Figure 7). The smaller SOA observed in the Dry_Ext group (Figure 5) may be due to physical processes present in the subtropics (e.g., dry air and subsidence) compared to physical processes present in the deep tropics (e.g., moist air and ascent) (Deng & Ritchie, 2018; Laing & Evans, 2016).

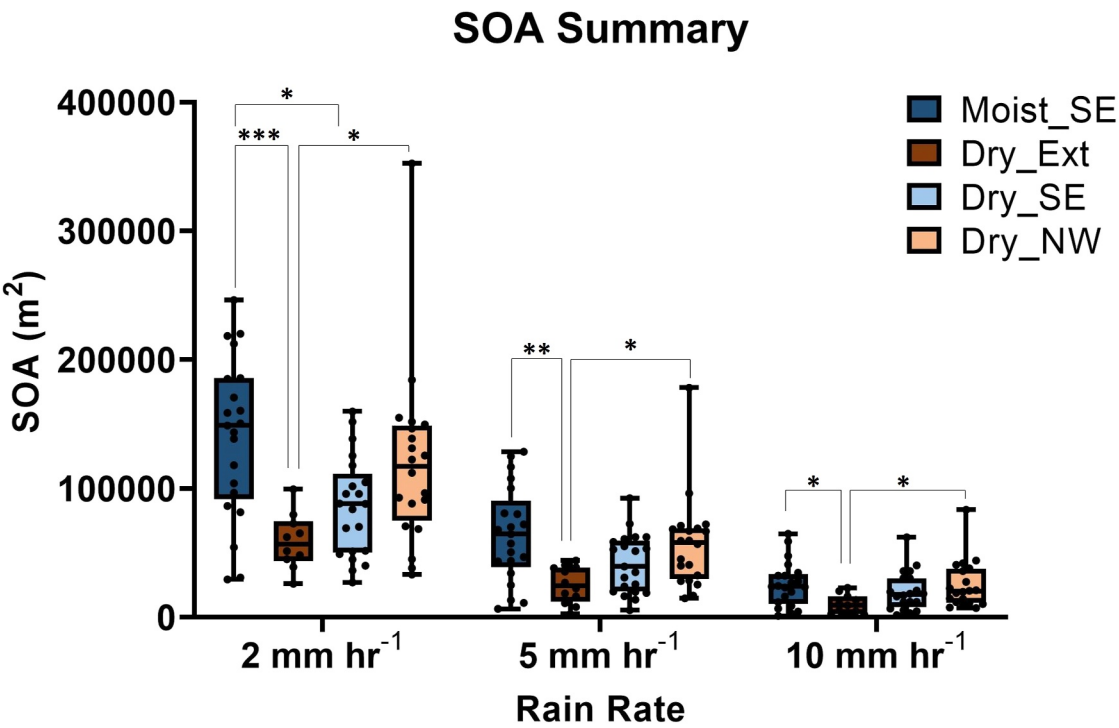

Figure 7. Same as Figure 6 but for box plots showing the precipitation areas for four moisture environments for 2, 5, and 10 mm hr^{-1} rain rate thresholds. The number of asterisks indicates statistical significance (*$p < 0.05$; **$p < 0.01$; ***$p < 0.001$).

4.2.2.2. Closure

Closure is evaluated over multiple radii spanning the inner core (C100), intermediary (C200), and outer regions (C300, C400, and C500). A higher closure in intermediary regions of the TC (100–200 km) is associated with a higher closure in the outer regions of the TC (300–500 km) (Table S1 in Supporting Information S1). A higher closure also typically aligns with a larger SOA especially at the 2 and 5 mm hr^{-1} rain rate thresholds (Table S1 in Supporting Information S1, Figure 7). Interestingly, there are no differences in closure among the groups for rainfall in the inner (C100) and intermediary (C200) regions of the TCs, which is the region where TCWV values were ignored for the EOF analysis. Lastly, there are no differences in closure between Moist_SE and Dry_NW, suggesting similar closure in the TC inner core and intermediate and outer regions (Figure 8). Interestingly, these two moisture patterns that have higher moisture located to the southeast of the TC, a location that could be favorable for TCs in low-moderate westerly shear (Ge et al., 2013).

Significant differences in closure occur primarily at the 2 mm hr^{-1} rain rate and in the outer rainband region ($r > 200$ km). TCs in the Moist_SE group are significantly more closed than TCs in the Dry_Ext group for the radial bins 200–300, 300–400, and 400–500 km from the TC center at all rain rates (Figure 8). For example, C300 (for radial bin 200–300 km) is higher in Hurricane Irma for the 2 and 5 mm hr^{-1} rain rates (Table 2) due to the outer rainbands extending to the northwest and southeast of the TC (Figure 3). At even larger radii, closure for radial bin 300–400 km (C400) and for radial bin 400–500 km (C500) is higher in Hurricane Irma for the 2 mm hr^{-1} rain rate (Table 2) due to the outer spiral rainband extending to the southeast of the TC (Figure 3). The results presented in Figure 8 demonstrate that rainbands are much more prevalent in the outer region ($r > 200$ km) for TCs in the Moist_SE group. Additionally, the Moist_SE group is significantly more closed than the Dry_SE group for the outer rainband region for radial bins 300–400 and 400–500 km from the TC center at the 2 and 5 mm hr^{-1} rain rates (Figures 8a and 8b) and for the radial bin 400–500 km from the TC center at the 10 mm hr^{-1} rain rate (Figure 8c). Lastly, the Dry_NW group is significantly more closed than the Dry_Ext group for the outer region 300–400 km radial bin at the 2 mm hr^{-1} rain rate (Figure 8a).

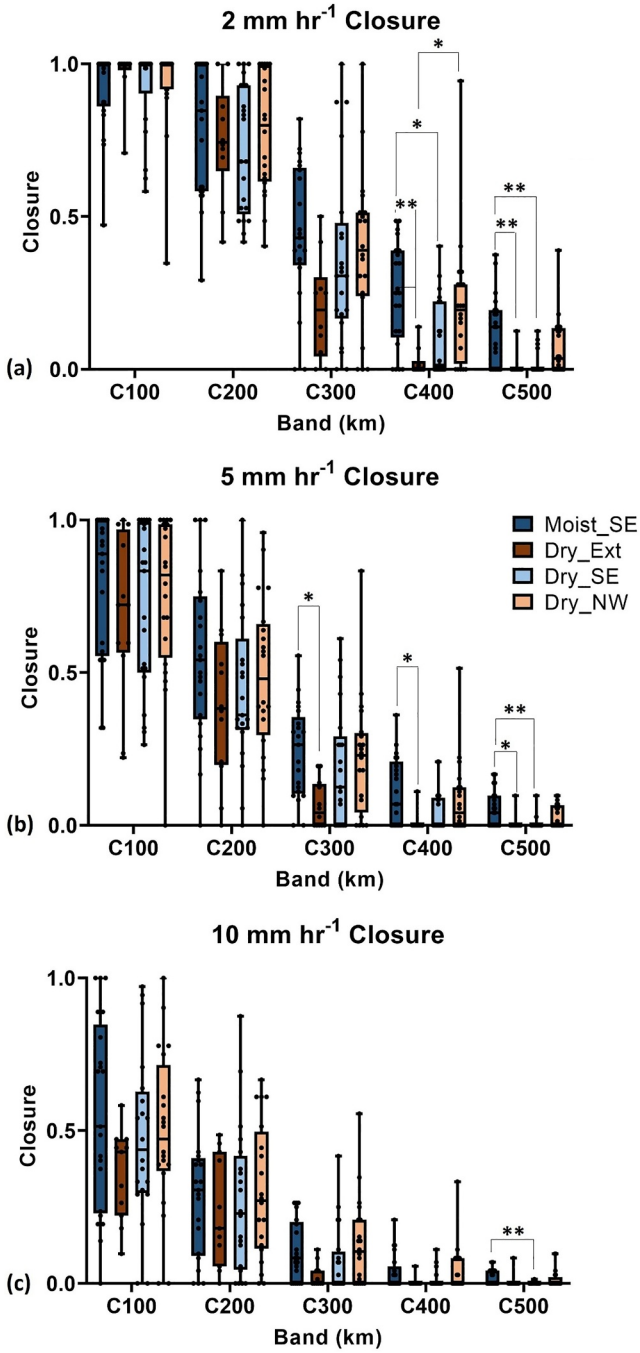

Figure 8. Same as Figure 6 but for the closure of precipitation regions for four moisture environments for (a) 2, (b) 5, and (c) 10 mm hr^{-1} rain rate thresholds. C100 represents 0–100 km to focus on the TC inner core; C200 represents 100–200 km to evaluate the intermediate region between the TC inner and outer core; and C300, C400, and C500 represent the 200–300, 300–400, and 400–500 km bins, respectively, to capture the TC outer core. The number of asterisks indicates statistical significance (*$p < 0.05$; **$p < 0.01$).

4.2.2.3. Solidity

As noted earlier, there is a relationship between the closure within various radial bins and the SOA of different rain rates. Most notably, the 5 and 10 mm hr^{-1} SOA is most associated with higher closure values in the inner and middle regions of the TC (Table S1 in Supporting Information S1). Solidity values across all groups appear similar; however, storms in the Moist_SE group are significantly less solid than those in the Dry_Ext group at the 2 mm hr^{-1} rain rate and those in the Dry_SE group at the 5 mm hr^{-1} rain rates (Figure 9). Such differences indicate that storms in the Dry_SE group have smaller but significantly more solid convective areas compared to storms in the Moist_SE group and that storms in the Dry_Ext group have smaller but significantly more solid areas of stratiform precipitation compared to storms in the Moist_SE group. Higher solidity may be related to less outer spiral banding and, as a result, a more compact storm (e.g., Figures 3c and 3d). Prior research has indicated that TCs in a moist environment generate more distant rainbands, which could contribute to solidity differences and an overall larger storm size when measuring size via rain rate (e.g., Hill & Lackmann, 2009; Zhou and Matyas, 2018).

4.2.2.4. Dispersion

Dispersion is moderately correlated with closure in the outer regions ($r > 200$ km) of the TC (Table S1 in Supporting Information S1). Despite the statistical relationships between the other shape metrics discussed in earlier sections, there are no significant differences in dispersion measures among moisture groups. Physically, the lack of significant differences suggests that stratiform precipitation is situated at similar distances from the TC center for all cases regardless of the moisture environment, and that convective precipitation is also situated at similar distances from the TC center, a result potentially related to our study's minimum intensity criteria (maximum wind speeds of at least 65 kt).

4.3. TC Evolution by Moisture Environment

When testing for statistical significance using the Kruskal Wallis test, few differences were significant among groups for TC intensity, intensity trend, size, and shape over the 48 hr we examined (Table 3). The only significant difference was the evolution of the 200-km closure for the 10 mm hr^{-1} rain rate for TCs in Moist_SE (Table 3, Figure 10). Though there are no clear differences in RMW (Table 3), the increase in closure for the 10 mm hr^{-1} rain rate (Figure 10) suggests more symmetric heating or a strengthening primary and secondary circulation (Kieper & Jiang, 2012). This idea is reflected in the slight drop in $MSLP_{min}$ and increase in maximum sustained winds (not shown) that are also observed at the beginning of the time window for the Moist_SE group (Figure 10).

Although there are no significant intensity or intensity trend differences among the groups, there is an intriguing difference in the percent of cases that undergo rapid intensification (RI) versus rapid weakening (RW) defined as a change of 30 knots or more within any 24 hr period that includes the sample time (Table 4). In general, there is more RI compared with RW in all the groups, potentially related to our data set being restricted to TCs with vertical wind shear below 20 kt. Note that TCs in the Moist_SE and Dry_NW groups have higher rates of RI, and there is only one RI event within the Dry_Ext group. The higher RI rate in the Moist_SE group is consistent with an increase in 10 mm hr^{-1} closure, but we do not find a similar increase in closure for TCs in the Dry_NW group,

Table 2
Closure Values for All Radial Bins and Rain Rates for Hurricane Irma (2017), a TC Sample in the Moist_SE Group, and Hurricane Gaston (2016), a TC Sample in the Dry_Ext Group (See Figure 3)

Storm name	Group	2 mm/hr C100	2 mm/hr C200	2 mm/hr C300	2 mm/hr C400	2 mm/hr C500
Irma (2017)	Moist_SE	1.0000	1.0000	0.6667	0.3889	0.0556
Gaston (2016)	Dry_Ext	1.0000	0.7361	0.0556	0.0000	0.0000
Storm Name	Group	5 mm/hr C100	5 mm/hr C200	5 mm/hr C300	5 mm/hr C400	5 mm/hr C500
Irma (2017)	Moist_SE	1.0000	0.2500	0.0972	0.0000	0.0000
Gaston (2016)	Dry_Ext	0.7500	0.5000	0.0000	0.0000	0.0000
Storm Name	Group	10 mm/hr C100	10 mm/hr C200	10 mm/hr C300	10 mm/hr C400	10 mm/hr C500
Irma (2017)	Moist_SE	0.8889	0.0000	0.0000	0.0000	0.0000
Gaston (2016)	Dry_Ext	0.5833	0.4028	0.0000	0.0000	0.0000

suggesting that increasing 100–200 km closure is not a requirement for RI. Here, we will note that 0–100 km closure is generally highest in the Moist_SE and Dry_NW groups and lowest in the Dry_Ext group (Figure 8c) in which there is only one case undergoing RI at the sample time. Therefore, higher closure rates in the inner core (0–100 km) and transition zone (100–200 km) regions of the TC may help to support RI, but an increase in closure is not associated with RI based on the TCs in this study.

4.4. Vertical Wind Shear

The TC samples explored in this study occur within environments with 200–800-km vertical wind shear ≤20 knots to control for one known influence on TC size and intensity. Given our findings on size and structure differences among the groups, we next consider vertical wind shear magnitude and direction to assess another potential reason for those differences. Note that we only include the results regarding shear magnitude since there

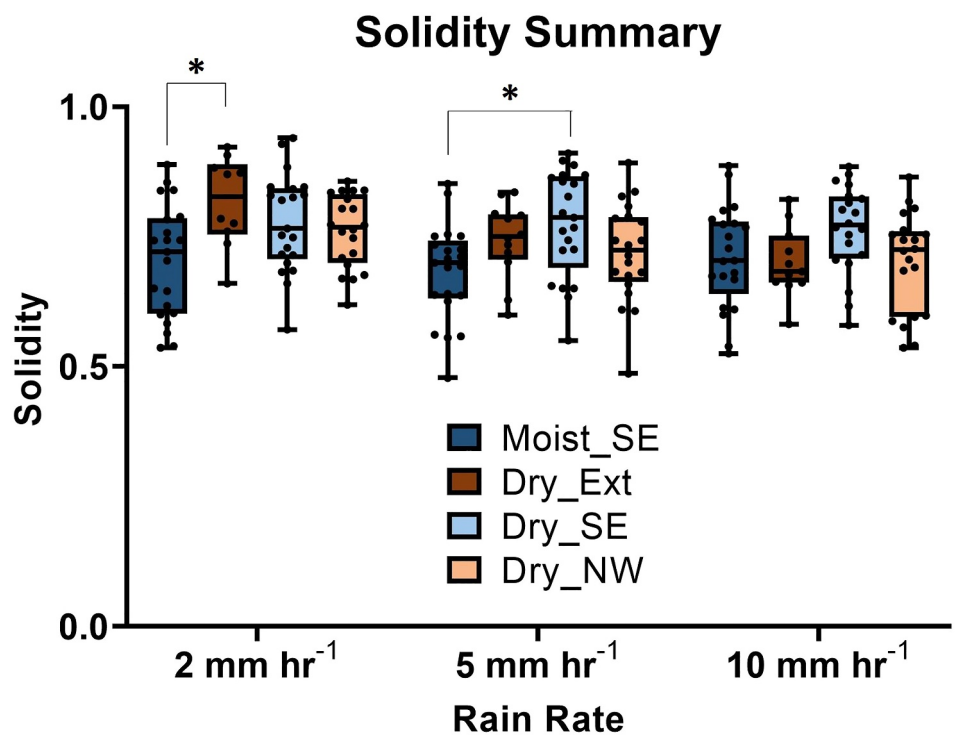

Figure 9. Same as Figure 5 but for solidity values for four moisture environments for 2, 5, and 10 mm hr^{-1} rain rate thresholds. The number of asterisks indicate statistical significance (*$p < 0.05$).

Table 3
Results From the Kruskal-Wallis Test (p-Values) for TC Size and Intensity Metrics and 10 mm Hr^{-1} Shape Metric Evolution

10 mm/hr	Moist_SE	Dry_Ext	Dry_SE	Dry_NW
Vmax	0.596	0.939	0.881	0.127
$MSLP_{min}$	0.371	0.975	0.871	0.200
ROCI	0.954	0.999	0.975	0.982
R34	0.615	0.972	0.689	0.561
R64	0.406	0.504	0.929	0.374
RMW	0.783	0.955	0.991	0.500
SOA	0.407	0.602	0.987	0.566
Solidity	0.552	0.400	0.657	0.303
Closure 100	0.647	0.544	0.438	0.889
Closure 200	***0.025***	0.136	0.634	0.958
Closure 300	0.994	0.528	0.980	0.216
Closure 400	0.980	0.241	0.725	0.242
Dispersion	0.945	0.576	0.396	0.572

were no significant differences in TC shape or size based on the shear direction (not shown). The distribution of shear magnitude values in each group (Figure 11) is generally similar based on the Kruskal Wallis test ($p = 0.525$). Although there appear to be minor differences among the moisture groups, including slightly weaker shear in the Moist_SE group, these differences are not statistically significant. This result indicates that differences in the TC precipitation structure among the groups are mainly related to the moisture environment.

Next, we evaluate the influence of shear magnitude on the TC size and shape metrics. We use Spearman's correlation coefficients (r) due to the relatively small sample size ($n = 75$) and non-normal distributions for some metrics (e.g., closure). Weak to moderate correlations are found for a few variables, including dispersion and closure at all three rain rates (Table 5). Collectively, these increases in dispersion and outer core (200–300 km and 300–400 km radial bins) closure suggest that higher wind shear leads to asymmetric precipitation that is displaced away from the TC center into outer regions of the TC. We speculate the moderate correlation between dispersion and outer core closure (Table S1 in Supporting Information S1) is due to TCs in the sample that experience moderate wind shear, leading to precipitation that is displaced from the TC center and, therefore, also located at larger radial distances from the TC center. Additionally, there is a positive correlation between VWS and latitude, indicating that wind shear increases with latitude as expected.

5. Conclusions

This study focuses on the following research question: how do precipitation patterns and wind field size differ among TCs in varying environmental moisture patterns? TCs included in the analysis are hurricanes (≥65 kt) located away from major landmasses in an area of low to moderate environmental vertical wind shear (≤20 kt). Common large-scale moisture environments surrounding Atlantic hurricanes are identified through EOF analysis (Moist_SE, Dry_Ext, Dry_SE, and Dry_NW), and cases that most contribute to each moisture (EOF) pattern are then explored. Geographically, samples in the Dry_Ext group are located significantly farther north into the subtropical North Atlantic compared to all other groups. Additionally, there are no Dry_SE cases located in the Gulf of Mexico or Caribbean Sea; instead, the majority of cases in these two regions were from the Moist_SE group. Longitudinal spread of cases in the Dry_NW and Moist_SE groups was nearly twice as large compared with cases in the Dry_Ext and Dry_SE groups.

Multiple spatial metrics are calculated and compared for rain rate (2, 5, and 10 mm hr^{-1}) regions associated with the sample TCs in the four moisture environments. We also compare TC size (based on the wind field and the rain field), intensity, time since genesis, and location among the groups. Additionally, we evaluate size and shape

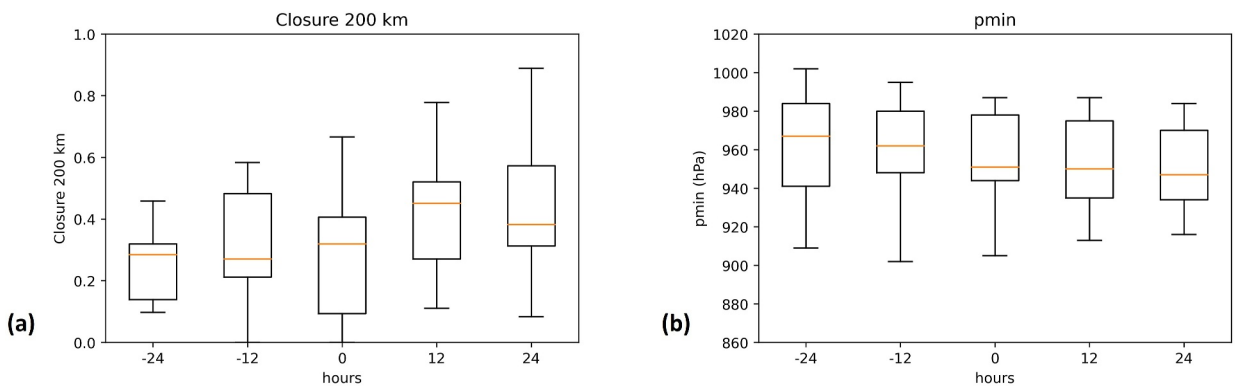

Figure 10. Box plots showing the evolution of the (a) 10 mm hr^{-1} C200 band and (b) MSLP for TCs in the Moist_SE group. All box plots display the median (in orange) and interquartile range (IQR). The whiskers extend from the edges of the box to show the range of the data but do not extend more than 1.5 × IQR.

Table 4
Percent [%] of Cases in Each Moisture Group That Undergo Rapid Intensification or Rapid Weakening Within Any 24 hr Period That Includes the Sample Time

	Moist_SE	Dry_Ext	Dry_SE	Dry_NW
RI	47.6	7.7	28.6	50.0
RW	9.5	0.0	4.8	10.0

metrics over a 48-hr window centered on the sample time to better understand how moisture environments influence TC evolution before and after the TC moves into that moisture environment. Although shear is limited by the original criteria, we perform an additional analysis to investigate the differences in TC size and shape between cases experiencing easterly and westerly shear.

Stratiform and convective rain areas in TCs in a more moist environment (Moist_SE) are generally larger with more enclosed rainbands than those rain areas in TCs in any other group, especially TCs in a comparatively dry environment (Dry_Ext). TCs in the Moist_SE group develop more enclosed rainbands in the 100–200 km radial bin and strengthen slightly in the 48-hr window surrounding the central time step. Additionally, stratiform and convective rain areas in TCs in overall drier environments (Dry_Ext) are significantly smaller than stratiform and convective rain areas in TCs with dry air to the northwest (Dry_NW). TCs in more moist environment (Moist_SE), while larger in terms of total stratiform and convective rain area, are significantly less compact or solid than those areas in TCs in drier environments (Dry_Ext and Dry_SE). Our results are in line with previous research showing that TCs in a moist environment have larger rain areas (Braun et al., 2012; Hill & Lackmann, 2009) and more rainbands in the TC outer core region (Hill & Lackmann, 2009; Kim et al., 2021).

Despite the precipitation structure differences among TCs in varied moisture environments, there are no significant differences in their inner and outer wind radii. This result does not align with findings from modeling and observational studies showing that TC wind field size is sensitive to environmental moisture (Braun et al., 2012; Hill & Lackmann, 2009; Kim et al., 2021; Matyas, 2017; Wu et al., 2015; Ying and Zhang, 2012). In fact, Matyas et al. (2025) find significant differences in R34 among the four moisture groups in their larger sample of TCs. Further analysis is needed to determine if our result is supported by other observational studies.

We speculate that the TCs in our study are impacted by multiple factors in addition to environmental moisture, such as the latitude and time since genesis. For example, TCs tend to form at low latitudes, where the Moist_SE and Dry_SE environments dominate, then move to higher latitudes, where the Dry_Ext environment dominates, which may help to explain the relatively large TC sizes in the Dry_Ext group given that TC wind field size

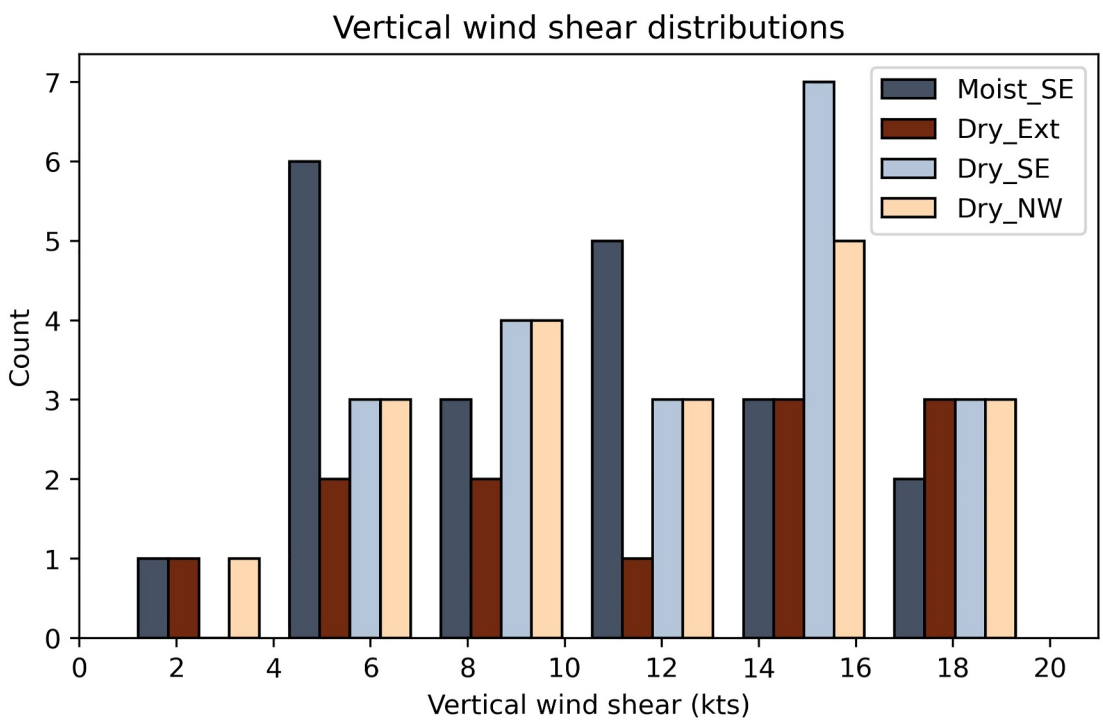

Figure 11. Histogram showing the distribution of shear magnitude (in knots) for each moisture group.

Table 5
Spearman's Correlation Coefficients and Associated p-Values for All Shape and Size Metrics Versus Vertical Wind Shear Magnitude

Variable	Spearman's r	p	Variable	Spearman's r	p
Time since genesis	0.13	0.276	10 mm/hr SOA	0.17	0.149
2 mm/hr SOA	0.2	0.101	10 mm/hr Solidity	0.04	0.719
2 mm/hr Solidity	−0.03	0.831	10 mm/hr C100	−0.12	0.315
2 mm/hr C100	−0.01	0.915	10 mm/hr C200	0.17	0.154
2 mm/hr C200	0	0.993	**10 mm/hr C300**	**0.27**	**0.021**
2 mm/hr C300	0.17	0.165	10 mm/hr C400	0.14	0.227
2 mm/hr C400	**0.3**	**0.01**	10 mm/hr C500	0.12	0.316
2 mm/hr C500	0.11	0.369	**10 mm/hr Dispersion**	**0.27**	**0.021**
2 mm/hr Dispersion	**0.25**	**0.031**	Maximum Sustained Winds (kts)	0.01	0.918
5 mm/hr SOA	0.19	0.113	MSLP (hPa)	−0.13	0.278
5 mm/hr Solidity	−0.01	0.962	RMW (nm)	0.12	0.301
5 mm/hr C100	−0.15	0.209	ROCI (nm)	0.14	0.232
5 mm/hr C200	0.03	0.777	R34 (nm)	0.2	0.092
5 mm/hr C300	**0.24**	**0.038**	R64 (nm)	0.13	0.252
5 mm/hr C400	**0.28**	**0.016**	**Latitude**	**0.33**	**0.003**
5 mm/hr C500	0.12	0.326	Longitude	−0.14	0.241
5 mm/hr Dispersion	**0.3**	**0.009**			

Note. Bolded values indicate significant relationships at a 95% confidence level.

generally increases with latitude (Knaff et al., 2014). Multiple studies show that TC outer size expands with time toward an equilibrium or potential size (Martinez et al., 2020; Wang & Chavas, 2024; Wang et al., 2022), stressing the importance of time since genesis as an important control on TC outer wind field size. Although environmental variables are important in estimating the size of the TC outer wind field (Wang et al., 2022), other variables such as the latitude and expansion with time (Knaff et al., 2014; Schenkel et al., 2018) are also important and may be dominating the results in this study. Additionally, it is notable that TC outer wind field size has not changed substantially in recent decades (Schenkel et al., 2023) despite marked increases in environmental moisture (Zarzycki et al., 2024), a result that might partially corroborate our finding of minimal differences in TC wind field size based on the moisture environment. Lastly, multiple studies find that the initial TC size is determined by the moisture environment during the formation stage (Braun et al., 2012; Hill & Lackmann, 2009; Martinez et al., 2020; Wu et al., 2015) and that TCs tend to maintain their initial size (small vs. large) over their lifecycle (Knaff et al., 2014). Our study does not consider the moisture environment at the time of genesis, which may be more important than the moisture environment at the sampling time. Collectively, our results suggest that there is still some uncertainty regarding the influence of large-scale moisture on the TC outer wind field size and that more research needs to be conducted to understand this problem better.

The results of this study are limited by satellite and model resolution as well as the precision of observational wind radii and wind speed data. Extended best track wind radii are estimated by forecasters, and uncertainty can be as high as 40%–45% for hurricane wind radii that are based only on satellite data (Landsea & Franklin, 2013). Since all of the cases in this study are TCs away from land, the quality of the TC wind radii may be degraded by a lack of observations. Next, in our study, the need to ensure independence among moisture groups reduces the number of cases in each group, which could limit the power of some statistical tests. For example, the TCs in this study are slightly smaller than the larger set of Atlantic TCs studied by Kimball and Mulekar (2004). This smaller range of wind radii in our TC cases may make it harder to find significant differences among the moisture environments, unlike the results by Matyas et al. (2025), and may be due to sampling or the other constraints we placed on shear and distance to land. Future work should consider using less stringent criteria in identifying cases for the moisture groups. Lastly, additional observational and idealized studies focused on the influence of varying moisture

environments on TC wind field size should be completed to determine if the current study's result showing no difference in TC wind field size based on the moisture enviroment is supported by theory and observations.

Data Availability Statement

Software used to produce the results in this manuscript is made accessible through the Virginia Tech Data Repository (https://data.lib.vt.edu) at https://doi.org/10.7294/27994187 (Zick et al., 2025) available under the CC0 1.0 license. All figures and tables in the manuscript are generated using Python 3.12.7, ArcGIS Pro, and GraphPad/Prism 10 (GraphPad Software, 2025). Figures were made with Matplotlib version 3.9.2 (Hunter, 2007; The Matplotlib Development Team, 2024) available under the Matplotlib license at https://matplotlib.org/. Shape metric analysis untilized the scikit-image image processing software (Walt et al., 2014) available under the liberal BSD Open Source license. Lastly, we used the *eofs* software package, a python package for computing empirical orthogonal functions (EOFs) (Dawson, 2016), available under the GNU General Public License Version 3. Public data sets include (a) the Atlantic hurricane database HURDAT2 (https://www.nhc.noaa.gov/data/#hurdat) (Landsea & Beven, 2019), (b) NASA's Global Precipitation Measurement IMERG final precipitation (https://catalog.data.gov/dataset/gpm-imerg-final-precipitation-l3-half-hourly-0-1-degree-x-0-1-degree-v07-gpm-3imerghh-at-g) (Huffman et al., 2020; NASA EarthData, 2024), (c) the Tropical Cyclone Extended Best Track Dataset (https://rammb2.cira.colostate.edu/research/tropical-cyclones/tc_extended_best_track_dataset/) (Demuth et al., 2006), (d) the European Centre for Medium-Range Weather Forecasts (ECMWF) atmospheric reanalysis (ERA5) (https://www.ecmwf.int/en/forecasts/datasets/reanalysis-datasets/era5) (Guillory, 2022; Hersbach et al., 2020) [Dataset], and (e) the Statistical Hurricane Intensity Prediction Scheme (SHIPS) data set (https://rammb.cira.colostate.edu/research/tropical_cyclones/ships/data/) (DeMaria & Kaplan, 1994).

Acknowledgments
This study was supported by the National Science Foundation (AGS- 2012008, 2011981, 2011812). We appreciate input from Kayleigh's MS committee members, Dr. Andrew Ellis and Dr. Anamaria Bukvic.

References

Aarons, Z. S., Camargo, S. J., Strong, J. D. O., & Murakami, H. (2021). Tropical cyclone characteristics in the MERRA-2 reanalysis and AMIP simulations. *Earth and Space Science*, *8*(3), e2020EA001415. https://doi.org/10.1029/2020EA001415

Alland, J. J., Tang, B. H., & Corbosiero, K. L. (2017). Effects of midlevel dry air on development of the axisymmetric tropical cyclone secondary circulation. *Journal of the Atmospheric Sciences*, *74*(5), 1455–1470. https://doi.org/10.1175/JAS-D-16-0271.1

Berislavich, K. (2023). An analysis of moisture environments associated with mature North Atlantic tropial cyclones. *Retrieved from WorldCat.org on December 8, 2024*. Mississippi State University.

Braun, S. A., Sippel, J. A., & Nolan, D. S. (2012). The impact of dry midlevel air on hurricane intensity in idealized simulations with No mean flow. *Journal of the Atmospheric Sciences*, *69*(1), 236–257. https://doi.org/10.1175/JAS-D-10-05007.1

Bytheway, J. L., & Kummerow, C. D. (2015). Toward an object-based assessment of high-resolution forecasts of long-lived convective precipitation in the central U.S. *Journal of Advances in Modeling Earth Systems*, *7*(3), 1248–1264. https://doi.org/10.1002/2015MS000497

Chan, K. T. F., & Chan, J. C. L. (2014). Impacts of initial vortex size and planetary vorticity on tropical cyclone size. *Quarterly Journal of the Royal Meteorological Society*, *140*(684), 2235–2248. https://doi.org/10.1002/qj.2292

Chan, K. T. F., & Chan, J. C. L. (2018). The outer-core wind structure of tropical cyclones. *Journal of the Meteorological Society of Japan. Ser. II*, *96*(4), 297–315. https://doi.org/10.2151/jmsj.2018-042

Chavas, D. R., & Emanuel, K. A. (2010). A QuikSCAT climatology of tropical cyclone size. *Geophysical Research Letters*, *37*(18). https://doi.org/10.1029/2010GL044558

Chavas, D. R., & Knaff, J. A. (2022). A simple model for predicting the tropical cyclone radius of maximum wind from outer size. *Weather and Forecasting*, *37*(5), 563–579. https://doi.org/10.1175/WAF-D-21-0103.1

Chavas, D. R., & Lin, N. (2016). A model for the complete radial structure of the tropical cyclone wind field. Part II: Wind field variability. *Journal of the Atmospheric Sciences*, *73*(8), 3093–3113. https://doi.org/10.1175/JAS-D-15-0185.1

Chavas, D. R., Lin, N., & Emanuel, K. (2015). A model for the complete radial structure of the tropical cyclone wind field. Part I: Comparison with observed structure. *Journal of the Atmospheric Sciences*, *72*(9), 3647–3662. https://doi.org/10.1175/JAS-D-15-0014.1

Chen, B.-F., Davis, C. A., & Kuo, Y.-H. (2021). Examination of the combined effect of deep-layer vertical shear direction and lower-tropospheric mean flow on tropical cyclone intensity and size based on the ERA5 reanalysis. *Monthly Weather Review*, *149*(12), 4057–4076. https://doi.org/10.1175/MWR-D-21-0120.1

Corbosiero, K. L., & Molinari, J. (2002). The effects of vertical wind shear on the distribution of convection in tropical cyclones. *Monthly Weather Review*, *130*(8), 2110–2123. https://doi.org/10.1175/1520-0493(2002)130<2110:TEOVWS>2.0.CO;2

Dawson, A. (2016). Eofs: A library for EOF analysis of meteorological, oceanographic, and climate data. JORS [Software]. *Zenodo*, *4*(1). https://doi.org/10.5334/jors.122.14

DeMaria, M., & Kaplan, J. (1994). A Statistical Hurricane Intensity Prediction Scheme (SHIPS) for the Atlantic basin [Dataset]. *Weather and Forecasting*, *9*(2), 209–220. https://doi.org/10.1175/1520-0434(1994)009<0209:ASHIPS>2.0.CO;2

Demuth, J. L., DeMaria, M., & Knaff, J. A. (2006). Improvement of Advanced Microwave Sounding Unit tropical cyclone intensity and size estimation algorithms [Dataset]. *Journal of Applied Meteorology and Climatology*, *45*(11), 1573–1581. https://doi.org/10.1175/JAM2429.1

Deng, D., & Ritchie, E. A. (2018). A metric for rainfall asymmetry in recurving tropical cyclones. *Geophysical Research Letters*, *45*(13), 6741–6749. https://doi.org/10.1029/2018GL078273

Dirkes, C. A., Wing, A. A., Camargo, S. J., & Kim, D. (2023). Process-oriented diagnosis of tropical cyclones in reanalyses using a moist static energy variance budget. *Journal of Climate*, *1*(aop), 1–52. https://doi.org/10.1175/JCLI-D-22-0384.1

Dunn, O. J. (1964). Multiple comparisons using rank sums. *Technometrics*, *6*(3), 241–252. https://doi.org/10.1080/00401706.1964.10490181

Feng, X., & Shu, S. (2018). How do weak tropical cyclones produce heavy rainfall when making landfall over China. *Journal of Geophysical Research: Atmospheres*, *123*(21), 11–848. https://doi.org/10.1029/2018JD029228

Frank, W. M., & Ritchie, E. A. (1999). Effects of environmental flow upon tropical cyclone structure. *Monthly Weather Review*, *127*(9), 2044–2061. https://doi.org/10.1175/1520-0493(1999)127<2044:EOEFUT>2.0.CO;2

Ge, X., Li, T., & Peng, M. (2013). Effects of vertical shears and midlevel dry air on tropical cyclone developments. *Journal of the Atmospheric Sciences*, *70*(12), 3859–3875. https://doi.org/10.1175/JAS-D-13-066.1

Gori, A., Lin, N., Schenkel, B., & Chavas, D. (2023). North Atlantic tropical cyclone size and storm surge reconstructions from 1950-present. *Journal of Geophysical Research: Atmospheres*, *128*(5), e2022JD037312. https://doi.org/10.1029/2022JD037312

GraphPad Software, L. L. C. (2025). Graphpad prism 9 statistics guide - Interpreting results: Kruskal-Wallis Test. Prism 8 User Guide [Software]. https://www.graphpad.com/guides/prism/latest/statistics/how_the_kruskal-wallis_test_works.htm

Guillory, A. (2022). ERA5. Ecmwf [Dataset]. https://www.ecmwf.int/en/forecasts/datasets/reanalysis-datasets/era5

Halverson, J. B., Simpson, J., Heymsfield, G., Pierce, H., Hock, T., & Ritchie, L. (2006). Warm core structure of hurricane Erin diagnosed from high altitude dropsondes during CAMEX-4. *Journal of the Atmospheric Sciences*, *63*(1), 309–324. https://doi.org/10.1175/JAS3596.1

Hannachi, A. (2004). A primer for EOF analysis of climate data.

Hannachi, A., Jolliffe, I. T., & Stephenson, D. B. (2007). Empirical orthogonal functions and related techniques in atmospheric science: A review. *International Journal of Climatology*, *27*(9), 1119–1152. https://doi.org/10.1002/joc.1499

Hersbach, H., Bell, B., Berrisford, P., Hirahara, S., Horányi, A., Muñoz-Sabater, J., et al. (2020). The ERA5 global reanalysis [Dataset]. *Quarterly Journal of the Royal Meteorological Society*, *146*(730), 1999–2049. https://doi.org/10.1002/qj.3803

Hill, K. A., & Lackmann, G. M. (2009). Influence of environmental humidity on tropical cyclone size. *Monthly Weather Review*, *137*(10), 3294–3315. https://doi.org/10.1175/2009MWR2679.1

Holland, G. J., & Merrill, R. T. (1984). On the dynamics of tropical cyclone structural changes. *Quarterly Journal of the Royal Meteorological Society*, *110*(465), 723–745. https://doi.org/10.1002/qj.49711046510

Huffman, G. J., Bolvin, D. T., Braithwaite, D., Hsu, K.-L., Joyce, R. J., Kidd, C., et al. (2020). Integrated multi-satellite Retrievals for the global precipitation Measurement (GPM) mission (IMERG). In V. Levizzani, C. Kidd, D. B. Kirschbaum, C. D. Kummerow, K. Nakamura, & F. J. Turk (Eds.), *Satellite precipitation Measurement. Advances in global change research* (Vol. 67, pp. 343–353). https://doi.org/10.1007/978-3-030-24568-9_19

Hunter, J. D. (2007). Matplotlib: A 2D graphics environment [Software]. *Computing in Science and Engineering*, *9*(3), 90–95. https://doi.org/10.1109/MCSE.2007.55

Irish, J. L., Resio, D. T., & Ratcliff, J. J. (2008). The influence of storm size on hurricane surge. *Journal of Physical Oceanography*, *38*(9), 2003–2013. https://doi.org/10.1175/2008JPO3727.1

Jiang, H., Halverson, J. B., Simpson, J., & Zipser, E. J. (2008). Hurricane "rainfall potential" derived from satellite observations aids overland rainfall prediction. *Journal of Applied Meteorology and Climatology*, *47*(4), 944–959. https://doi.org/10.1175/2007jamc1619.1

Kieper, M. E., & Jiang, H. (2012). Predicting tropical cyclone rapid intensification using the 37 GHz ring pattern identified from passive microwave measurements. *Geophysical Research Letters*, *39*(13). https://doi.org/10.1029/2012GL052115

Kim, D., Ho, C.-H., Murakami, H., & Park, D.-S. R. (2021). Assessing the influence of large-scale environmental conditions on the rainfall structure of Atlantic tropical cyclones: An observational study. *Journal of Climate*, *34*(6), 2093–2106. https://doi.org/10.1175/JCLI-D-20-0376.1

Kimball, S. K., & Mulekar, M. S. (2004). A 15-Year climatology of North Atlantic tropical cyclones. Part I: Size parameters. *Journal of Climate*, *17*(18), 3555–3575. https://doi.org/10.1175/1520-0442(2004)017<3555:AYCONA>2.0.CO;2

Kirkland, J. L., & Zick, S. E. (2019). Regional differences in the spatial patterns of North Atlantic tropical cyclone rainbands through landfall. *Southeastern Geographer*, *59*(3), 294–320. https://doi.org/10.1353/sgo.2019.0023

Klotzbach, P. J., Bell, M. M., Bowen, S. G., Gibney, E. J., Knapp, K. R., & Schreck, C. J. (2020). Surface pressure a more skillful predictor of normalized hurricane damage than maximum sustained wind. *Bulletin of the American Meteorological Society*, *101*(6), E830–E846. https://doi.org/10.1175/BAMS-D-19-0062.1

Knaff, J. A., Longmore, S. P., & Molenar, D. A. (2014). An objective satellite-based tropical cyclone size climatology. *Journal of Climate*, *27*(1), 455–476. https://doi.org/10.1175/JCLI-D-13-00096.1

Kruskal, W. H., & Wallis, W. A. (1952). Use of ranks in one-criterion variance analysis. *Journal of the American Statistical Association*, *47*(260), 583–621. https://doi.org/10.1080/01621459.1952.10483441

Laing, A., & Evans, J.-L. (2016). A comprehensive online and print textbook. In *Produced by the COMET® program, university corporation for atmospheric research, version 4.0, March 2016* (2nd ed.). Introduction to Tropical Meteorology. Retrieved from https://www.meted.ucar.edu/tropical/textbook_2nd_edition/

Landsea, C., & Beven, J. (2019). The revised Atlantic hurricane database (HURDAT2) [Dataset]. https://www.aoml.noaa.gov/hrd/hurdat/hurdat2-format.pdf

Landsea, C. W., & Franklin, J. L. (2013). Atlantic hurricane database uncertainty and presentation of a new database format. *Monthly Weather Review*, *141*(10), 3576–3592. https://doi.org/10.1175/MWR-D-12-00254.1

Lau, K. M., & Wu, H. T. (2003). Warm rain processes over tropical oceans and climate implications. *Geophysical Research Letters*, *30*(24). https://doi.org/10.1029/2003GL018567

Li, R., Qi, D., Zhang, Y., & Wang, K. (2022). A new pixel-to-object method for evaluating the capability of the GPM IMERG product to quantify precipitation systems. *Journal of Hydrology*, *613*, 128476. https://doi.org/10.1016/j.jhydrol.2022.128476

Lonfat, M., Marks, F. D., & Chen, S. S. (2004). Precipitation distribution in tropical cyclones using the Tropical Rainfall Measuring Mission (TRMM) microwave imager: A global perspective. *Monthly Weather Review*, *132*(7), 1645–1660. https://doi.org/10.1175/1520-0493(2004)132<1645:PDITCU>2.0.CO;2

Martinez, J., Nam, C. C., & Bell, M. M. (2020). On the contributions of incipient vortex circulation and environmental moisture to tropical cyclone expansion. *Journal of Geophysical Research: Atmospheres*, *125*(21), e2020JD033324. https://doi.org/10.1029/2020JD033324

Matyas, C. (2017). Comparing the spatial patterns of rainfall and atmospheric moisture among tropical cyclones having a track similar to hurricane Irene (2011). *Atmosphere*, *8*(9), 165. https://doi.org/10.3390/atmos8090165

Matyas, C., Kim, D., Zick, S., & Wood, K. (2025). Four moisture patterns surrounding Atlantic hurricanes revealed by deep learning: Their characteristics and relationship with hurricane intensity and precipitation. *Atmospheric Research*, *322*, 108114. https://doi.org/10.1016/j.atmosres.2025.108114

Matyas, C., & Tang, J. (2019). Measuring radial and tangential changes in tropical cyclone rain fields using metrics of dispersion and closure. *Advances in Meteorology*, *2019*, e8614014. https://doi.org/10.1155/2019/8613943

Matyas, C., Zick, S. E., & Tang, J. (2018). Using an object-based approach to quantify the spatial structure of reflectivity regions in hurricane Isabel (2003). Part I: Comparisons between radar observations and model simulations. *Monthly Weather Review*, *146*(5), 1319–1340. https://doi.org/10.1175/MWR-D-17-0077.1

Matyas, C. J. (2010). Associations between the size of hurricane rain fields at landfall and their surrounding environments. *Meteorology and Atmospheric Physics*, *106*(3–4), 135–148. https://doi.org/10.1007/s00703-009-0056-1

Murakami, H. (2014). Tropical cyclones in reanalysis data sets. *Geophysical Research Letters*, *41*(6), 2133–2141. https://doi.org/10.1002/2014GL059519

NASA EarthData. (2024). GPM IMERG final precipitation L3 half hourly 0.1 degree x 0.1 degree V06. *Data*. Retrieved from https://catalog.data.gov/dataset/gpm-imerg-final-precipitation-l3-half-hourly-0-1-degree-x-0-1-degree-v07-gpm-3imerghh-at-g

NOAA Office for Coastal Management. (2022). Economics and Demographics. Retrieved from https://coast.noaa.gov/states/fast-facts/economics-and-demographics.html

North, G. R., Bell, T. L., Cahalan, R. F., & Moeng, F. J. (1982). Sampling errors in the estimation of empirical orthogonal functions. *Monthly Weather Review*, *110*(7), 699–706. https://doi.org/10.1175/1520-0493(1982)110<0699:SEITEO>2.0.CO;2

Powell, M. D., & Reinhold, T. A. (2007). Tropical cyclone destructive potential by integrated Kinetic energy. *Bulletin of the American Meteorological Society*, *88*(4), 513–526. https://doi.org/10.1175/BAMS-88-4-513

Reasor, P. D., Montgomery, M. T., & Grasso, L. D. (2004). A new look at the problem of tropical cyclones in vertical shear flow: Vortex resiliency. *Journal of the Atmospheric Sciences*, *61*(1), 3–22. https://doi.org/10.1175/1520-0469(2004)061<0003:ANLATP>2.0.CO;2

Regional and Mesoscale Meteorology Branch. (2022). The tropical cyclone Extended Best Track Dataset (EBTRK). March 2022 [Dataset]. https://rammb2.cira.colostate.edu/research/tropical-cyclones/tc_extended_best_track_dataset/

Riemer, M., & Laliberté, F. (2015). Secondary circulation of tropical cyclones in vertical wind shear: Lagrangian diagnostic and pathways of environmental interaction. *Journal of the Atmospheric Sciences*, *72*(9), 3517–3536. https://doi.org/10.1175/JAS-D-14-0350.1

Rios-Berrios, R., & Torn, R. D. (2017). Climatological analysis of tropical cyclone intensity changes under moderate vertical wind shear. *Monthly Weather Review*, *145*(5), 1717–1738. https://doi.org/10.1175/MWR-D-16-0350.1

Rios Gaona, M. F., Villarini, G., Zhang, W., & Vecchi, G. A. (2018). The added value of IMERG in characterizing rainfall in tropical cyclones. *Atmospheric Research*, *209*, 95–102. https://doi.org/10.1016/j.atmosres.2018.03.008

Rogers, R., Reasor, P., & Lorsolo, S. (2013). Airborne Doppler observations of the inner-core structural differences between intensifying and steady-state tropical cyclones. *Monthly Weather Review*, *141*(9), 2970–2991. https://doi.org/10.1175/MWR-D-12-00357.1

Ruan, Z., & Wu, Q. (2022). Relationship between size and intensity in North Atlantic tropical cyclones with steady radii of maximum wind. *Geophysical Research Letters*, *49*(3), e2021GL095632. https://doi.org/10.1029/2021GL095632

Schenkel, B. A., Chavas, D., Lin, N., Knutson, T., Vecchi, G., & Brammer, A. (2023). North Atlantic tropical cyclone outer size and structure remain unchanged by the late twenty-first century. *Journal of Climate*, *36*(2), 359–382. https://doi.org/10.1175/JCLI-D-22-0066.1

Schenkel, B. A., & Hart, R. E. (2012). An examination of tropical cyclone position, intensity, and intensity life cycle within atmospheric reanalysis datasets. *Journal of Climate*, *25*(10), 3453–3475. https://doi.org/10.1175/2011JCLI4208.1

Schenkel, B. A., Lin, N., Chavas, D., Oppenheimer, M., & Brammer, A. (2017). Evaluating outer tropical cyclone size in reanalysis datasets using QuikSCAT data. *Journal of Climate*, *30*(21), 8745–8762doi. https://doi.org/10.1175/JCLI-D-17-0122.1

Schenkel, B. A., Lin, N., Chavas, D., Vecchi, G. A., Oppenheimer, M., & Brammer, A. (2018). Lifetime evolution of outer tropical cyclone size and structure as diagnosed from reanalysis and climate model data. *Journal of Climate*, *31*(19), 7985–8004. https://doi.org/10.1175/JCLI-D-17-0630.1

Schumacher, C., & Houze, R. A. (2003). Stratiform rain in the tropics as seen by the TRMM precipitation radar. *Journal of Climate*, *16*(11), 1739–1756. https://doi.org/10.1175/1520-0442(2003)016<1739:SRITTA>2.0.CO;2

Shapiro, L. J., & Willoughby, H. E. (1982). The response of balanced hurricanes to local-sources of heat and momentum. *Journal of the Atmospheric Sciences*, *39*(2), 378–394. https://doi.org/10.1175/1520-0469(1982)039<0378:trobht>2.0.co;2

Ships Predictor Files - Colorado State University. (2022). Statistical tropical cyclone intensity forecast technique development [Dataset]. https://rammb.cira.colostate.edu/research/tropical_cyclones/ships/data/ships_predictor_file_2022.pdf

Slocum, C. J., Razin, M. N., Knaff, J. A., & Stow, J. P. (2022). Does ERA5 mark a new era for resolving the tropical cyclone environment? *Journal of Climate*, *35*(21), 3547–3564. https://doi.org/10.1175/JCLI-D-22-0127.1

Stackhouse, S. D., Zick, S. E., Matyas, C. J., Wood, K. M., Hazelton, A. T., & Alaka, G. J. (2023). Evaluation of experimental high-resolution model forecasts of tropical cyclone precipitation using object-based metrics. *Weather and Forecasting*, *38*(10), 2111–2134. https://doi.org/10.1175/WAF-D-22-0223.1

Tang, B., & Emanuel, K. (2010). Midlevel ventilation's constraint on tropical cyclone intensity. *Journal of the Atmospheric Sciences*, *67*(6), 1817–1830. https://doi.org/10.1175/2010JAS3318.1

The Matplotlib Development Team. (2024). Matplotlib: Visualization with Python (v3.9.2) [Software]. *Zenodo*. https://doi.org/10.5281/zenodo.13308876

Tokay, A., Short, D. A., Williams, C. R., Ecklund, W. L., & Gage, K. S. (1999). Tropical rainfall associated with convective and stratiform clouds: Intercomparison of disdrometer and profiler measurements. *Journal of Applied Meteorology and Climatology*, *38*(3), 302–320. https://doi.org/10.1175/1520-0450(1999)038<0302:TRAWCA>2.0.CO;2

Trabing, B. C., & Bell, M. M. (2020). Understanding error distributions of hurricane intensity forecasts during rapid intensity changes. *Weather and Forecasting*, *35*(6), 2219–2234. https://doi.org/10.1175/WAF-D-19-0253.1

van der Walt, S., Schönberger, J. L., Nunez-Iglesias, J., Boulogne, F., Warner, J. D., Yager, N., et al. (2014). Scikit-image: Image processing in Python [Software]. *PeerJ*, *2*, e453. https://doi.org/10.7717/peerj.453

Wang, D., & Chavas, D. R. (2024). An analytical model for tropical cyclone outer-size expansion on the f plane. *Journal of the Atmospheric Sciences*, *81*(7), 1097–1125. https://doi.org/10.1175/JAS-D-23-0088.1

Wang, D., Lin, Y., & Chavas, D. R. (2022). Tropical cyclone potential size. *Journal of the Atmospheric Sciences*, *1*(aop), 3001–3025. https://doi.org/10.1175/JAS-D-21-0325.1

Wang, S., & Toumi, R. (2016). On the relationship between hurricane cost and the integrated wind profile. *Environmental Research Letters*, *11*(11), 114005. https://doi.org/10.1088/1748-9326/11/11/114005

Wang, S., & Toumi, R. (2019). Impact of dry midlevel air on the tropical cyclone outer circulation. *Journal of the Atmospheric Sciences*, *76*(6), 1809–1826. https://doi.org/10.1175/JAS-D-18-0302.1

Weatherford, C. L., & Gray, W. M. (1988a). Typhoon structure as revealed by aircraft reconnaissance. Part I: Data analysis and climatology. *Monthly Weather Review*, *116*(5), 1032–1043. https://doi.org/10.1175/1520-0493(1988)116<1032:TSARBA>2.0.CO;2

Weatherford, C. L., & Gray, W. M. (1988b). Typhoon structure as revealed by aircraft reconnaissance. Part II: Structural variability. *Monthly Weather Review*, *116*(5), 1044–1056. https://doi.org/10.1175/1520-0493(1988)116<1044:TSARBA>2.0.CO;2

Wilks, D. (2011). *Frequent statistical inference nonparametric tests,* statistical Methods in the atmospheric sciences (pp. 158–177). Elsevier.

Wu, L., Su, H., Fovell, R. G., Dunkerton, T. J., Wang, Z., & Kahn, B. H. (2015). Impact of environmental moisture on tropical cyclone intensification. *Atmospheric Chemistry and Physics*, *15*(24), 14041–14053. https://doi.org/10.5194/acp-15-14041-2015

Ying, Y., & Zhang, Q. (2012). A modeling study on tropical cyclone structural changes in response to ambient moisture variations. *Journal of the Meteorological Society of Japan. Ser. II*, *90*(5), 755–770. https://doi.org/10.2151/jmsj.2012-512

Zarzycki, C. M., Zhang, T., Jones, A. D., Rastogi, D., Vahmani, P., & Ullrich, P. A. (2024). Changes in four decades of near-CONUS tropical cyclones in an ensemble of 12 km thermodynamic global warming simulations. *Geophysical Research Letters*, *51*(18), e2024GL110535. https://doi.org/10.1029/2024GL110535

Zhou, Y., & Matyas, C. J. (2018). Spatial characteristics of rain fields associated with tropical cyclones landfalling over the western Gulf of Mexico and Caribbean Sea. *Journal of Applied Meteorology and Climatology*, *57*(8), 1711–1727. https://doi.org/10.1175/jamc-d-18-0034.1

Zick, S., Matyas, C., Lackmann, G., Tang, J., & Bennett, B. (2022). Illustration of an object-based approach to identify structural differences in tropical cyclone wind fields. *Quarterly Journal of the Royal Meteorological Society*, *148*(746), 2587–2606. https://doi.org/10.1002/qj.4326

Zick, S. E., & Matyas, C. J. (2015a). Tropical cyclones in the North American Regional Reanalysis: An assessment of spatial biases in location, intensity, and structure. *Journal of Geophysical Research: Atmospheres*, *120*(5), 1651–1669. https://doi.org/10.1002/2014JD022417

Zick, S. E., & Matyas, C. J. (2015b). Tropical cyclones in the North American Regional Reanalysis: The impact of satellite-derived precipitation over ocean. *Journal of Geophysical Research: Atmospheres*, *120*(17), 8724–8742. https://doi.org/10.1002/2015JD023722

Zick, S. E., & Matyas, C. J. (2016). A shape metric methodology for studying the evolving geometries of synoptic-scale precipitation patterns in tropical cyclones. *Annals of the Association of American Geographers*, *106*(6), 1217–1235. https://doi.org/10.1080/24694452.2016.1206460

Zick, S. E., Wood, K. M., & Addington, K. (2025). Software and data for variations in tropical cyclone size and rainfall patterns based on synoptic-scale moisture environments in the North Atlantic [Software]. *University Libraries, Virginia Tech*. https://doi.org/10.7294/27994187